Coordinating Feedback and Switching for Control of Hybrid Nonlinear Processes

Nael H. El-Farra and Panagiotis D. Christofides
Dept. of Chemical Engineering, University of California, Los Angeles, CA 90095

A robust hybrid control strategy for a broad class of hybrid nonlinear processes with actuator constraints and uncertain dynamics is proposed. These variable-structure processes comprise a finite family of constrained uncertain continuous nonlinear dynamical subsystems, together with discrete events that trigger the transition between the continuous subsystems. The proposed control strategy is predicated on the idea of coordinating the hierarchical tasks of lower-level feedback-controller synthesis and upper-level switching logic design. Using multiple Lyapunov functions, a family of bounded robust, nonlinear feedback controllers are initially designed to robustly stabilize the constituent modes of the hybrid process, subject to uncertainty and constraints. The region of guaranteed closed-loop stability is then explicitly characterized for each mode in terms of the magnitude of actuator constraints and the size of the uncertainty. A set of stabilizing switching laws that track the energy evolution of the constituent modes are then derived to orchestrate safe transitions between the stability regions of the constituent modes and their respective controllers, in a way that respects actuator constraints and guarantees robust stability of the overall uncertain hybrid closed-loop system. This hybrid control method is applied through computer simulations to robustly stabilize an exothermic chemical reactor with switched dynamics, model uncertainty, and actuator constraints at an unstable steady-state and to design a fault-tolerant control system for chemical reactors through switching between multiple constrained control configurations.

Introduction

Traditionally, most of the research work in process control has been concerned predominantly with the control of continuous dynamic processes described by ordinary differential equations. Yet, there are numerous examples in the chemical process industries where the dynamical properties of the process depend rather on an intricate interaction between discrete and continuous variables. These are referred to as hybrid processes because they combine both continuous dynamics and discrete events. In many of these applications, the continuous behavior arises as a manifestation of the underlying physical laws governing the process, such as momentum, mass, and energy conservation, and is modeled by continuous-time differential equations. Discrete behavior, on the other hand, is ubiquitously multifaceted and can originate from a variety of sources, including (1) inherent physicochemical discontinuities in the continuous process dynamics, such as phase changes, flow reversals, shocks, and transitions; (2) the use of measurement sensors and control actuators with discrete settings/positions (such as binary sensors, on/off valves, pumps, heatings with constant current, motors with speed control); and (3) the use of logic-based switching for supervisory and safety control tasks.

Another common source of hybrid behavior in chemical processes comes from the interaction of the process with its operating environment. Changes in raw materials, energy sources, and product specifications, together with fluctuations in market demands, forecasts, and the concomitant adjustments in management decisions, lead invariably to the superposition of discrete events on the basically continuous process dynamics, in the form of controlled transitions between different operational regimes. Regardless of whether the hybrid (combined discrete–continuous) behavior arises as an inherent feature of the process itself, its operation, or its

Correspondence concerning this article should be addressed to P. D. Christofides.

control system, the overall process behavior in all of these instances is characterized by structurally different dynamics in different situations (modes/regimes), and is, therefore, more appropriately viewed as intervals of piecewise-continuous behavior (corresponding to material and energy flows) interspersed by discrete transitions governed by a higher-level decision-making entity.

The traditional approach of dealing with these systems in many areas of industrial control has been to separate the continuous control from the discrete control. In recent years, however, it has become increasingly evident that the interaction of discrete events with even simple continuous dynamics can lead to complex unpredictable dynamics and, consequently, to very undesirable outcomes (particularly in safety-critical applications) if not explicitly accounted for in the control-system design. As efficient and profitable process operation becomes more dependent on the control system, the need to design flexible, reliable, and effective control systems that can explicitly handle the intermixture of continuous and discrete dynamics, is increasingly apparent. Such flexibility and responsiveness play a critical role in achieving optimum production rates, high-quality products, minimizing waste to the environment, and operating as efficiently as possible. These considerations, together with the abundance of hybrid phenomena in chemical processes, provide a strong motivation for the development of analytical tools and systematic methods for the analysis and control of these systems in a way that explicitly captures the combined discrete–continuous interactions and their effects.

Even though tools for the analysis and control of purely continuous-time processes exist and, to a large extent, are well developed, similar techniques for combined discrete–continuous systems are limited at present, primarily due to the difficulty of extending the available concepts and tools to account for the hybrid nature of these systems and their changing dynamics, which makes them more difficult to describe, analyze, or control. These challenges, coupled with the abundance of hybrid phenomena in many engineering systems in general, have fostered a large and growing body of research work on a diverse array of problems, including the modeling (for example, Barton and Pantelides, 1994; Yamalidou and Kantor, 1990), simulation (for example, Barton and Pantelides, 1994), optimization (for example, Grossmann et al., 2001), stability analysis (for example, DeCarlo et al., 2001; Hespanha and Morse, 1999), and control (for example, Bemporad and Morari, 1999; Engell et al., 2000; Hu et al., 1999; Koutsoukos et al., 2000), of several classes of hybrid systems. Continued progress notwithstanding, important theoretical, and practical problems remain to be addressed in this area, such as the development of a unified and practical approach for control, which deals effectively with the copresence of strong nonlinearities in the continuous dynamics, model uncertainty, actuator constraints, and combined discrete–continuous interactions.

In a previous work (El-Farra and Christofides, 2001a, 2002), we developed a hybrid nonlinear control methodology for a broad class of switched nonlinear systems with input constraints. These are systems that consist of a finite family of continuous nonlinear dynamical modes, subject to hard constraints on their manipulated inputs, together with a higher-level supervisor that governs the transitions between the constituent modes. The key feature of the proposed control methodology was the integrated synthesis, via multiple Lyapunov functions (MLFs), of (1) lower-level feedback controllers that stabilize the constituent constrained modes and provide, simultaneously, an explicit characterization of the stability region for each mode, and (2) upper-level switching laws that orchestrate the transitions between the continuous modes and their respective controllers, in a way that ensures stability of the overall switched closed-loop system despite its constrained and changing dynamics.

In this article, we extend the scope and methodology of our previous work to deal with switched nonlinear processes whose dynamics are both constrained and uncertain. Typical sources of uncertainty in chemical processes include plant–model mismatch (such as modeling errors, unknown process parameters) as well as time-varying exogenous disturbances which, if not accounted for, can lead to significant deterioration in performance and even to closed-loop instability. For hybrid processes, the impact of model uncertainty transcends the well-known adverse effects on the stability and performance of purely continuous processes (which comprise in this case the lower-level modes of the hybrid process), since uncertainty also impacts on the design of the higher-level switching logic. Owing to the limitations imposed by actuator constraints on the stability regions of the constituent modes of the hybrid process, the design of a stabilizing switching scheme requires knowledge of these stability regions, in order to decide when (or where, in the state space) a particular mode can be activated. However, when plant–model discrepancies are taken into consideration, the actual stability region of each mode can be quite different from the one obtained under nominal conditions. Consequently, nominal characterizations of stability regions can no longer guarantee safe mode switching, and the switching rules need to be modified. To address these problems, we propose in this work a robust nonlinear hybrid control methodology that uses multiple robust control Lyapunov functions to (1) synthesize a family of robust bounded nonlinear feedback controllers that enforce robust stability in the constituent constrained uncertain modes; (2) explicitly characterize the stability region for each mode under uncertainty and constraints; and (3) design robust switching laws that coordinate safe transitions between the modes in a way that guarantees closed-loop stability of the overall switched closed-loop system. The proposed hybrid control method is applied, through computer simulations, to (1) robustly stabilize an exothermic chemical reactor, with switched dynamics, model uncertainty, and actuator constraints, at an unstable steady state, and (2) design a fault-tolerant control system for chemical reactors, through switching between multiple constrained control configurations.

Switched Nonlinear Processes with Uncertain Dynamics

State-space description

We consider the class of switched uncertain nonlinear processes described by the following state-space representation

$$\dot{x}(t) = f_{\sigma(t)}(x(t)) + G_{\sigma(t)}(x(t))u_{\sigma(t)} + W_{\sigma(t)}(x(t))\theta_{\sigma(t)}(t)$$
$$\sigma(t) \in \mathcal{I} = \{1, \ldots, N\} \qquad (1)$$

where $x(t) \in \mathbb{R}^n$ denotes the vector of continuous process

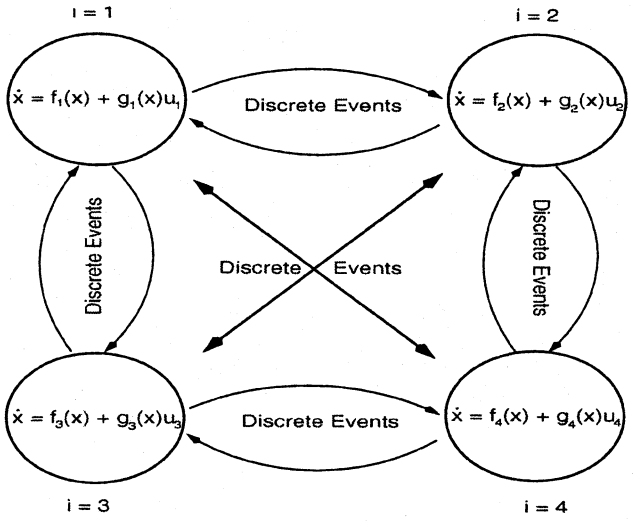

Figure 1. Multimodal hybrid process involving a finite family of continuous subsystems and discrete events governing their transitions.

state variables, $u(t) = [u^1(t) \cdots u^m(t)]^T \in \mathfrak{U} \subset \mathbb{R}^m$ denotes the vector of control inputs taking values in a nonempty compact convex subset of $\mathbb{R}^m$ that contains the origin in its interior, $\theta(t) = [\theta^1(t) \cdots \theta^q(t)]^T \in \Theta \subset \mathbb{R}^q$ denotes the vector of uncertain (possibly time-varying), but bounded, variables taking values in a nonempty compact convex subset of $\mathbb{R}^q$. The uncertain variables $\theta(t)$ may describe time-varying parametric uncertainty and/or exogenous disturbances. The switching signal, $\sigma: [0,\infty) \to \mathfrak{I}$ is assumed to be a piecewise continuous (from the right) function of time, implying that only a finite number of switches is allowed on any finite interval of time. The variable $\sigma(t)$, which takes values in the finite index set $\mathfrak{I}$, is a discrete state that indexes the vector field $f(\cdot)$, the matrices $G(\cdot)$ and $W(\cdot)$, the control input $u(\cdot)$, and the uncertain variable $\theta(\cdot)$, which altogether determine $\dot{x}$. For each value that the discrete state σ assumes in $\mathfrak{I}$, the temporal evolution of the continuous state, x, is governed by a different set of differential equations. Processes of the form of Eq. 1 are therefore of variable structure; they consist of a finite family of N continuous-time uncertain nonlinear subsystems (or modes) and some rules for switching between them (see Figure 1 for a graphical representation). These rules define a switching sequence that describes the temporal evolution of the discrete state. Note that, by indexing the vector of uncertain variables, $\theta(t)$, and the matrix $W(x)$ in Eq. 1 by σ, it is implied that the constituent modes do not necessarily share the same uncertain variables, nor are they equally affected by them. The uncertainty is, therefore, allowed to influence the dynamics of different modes differently.

Throughout the article, the notation t_{i_k} and $t_{i'_k}$ is used to denote the kth times that the ith subsystem is switched in and out, respectively, that is, $\sigma(t_{i_k}^+) = \sigma(t_{i'_k}^-) = i$, for all $k \in Z_+$. With this notation, it is understood that, when the ith mode is active, the continuous state evolves according to $\dot{x} = f_i(x) + G_i(x)u_i + W_i(x)\theta_i$ for $t_{i_k} \le t < t_{i'_k}$. It is assumed that all entries of the vector functions $f_i(x)$, the $n \times m$ matrices $G_i(x)$, the $n \times q$ matrices $W_i(x)$ are sufficiently smooth on $\mathbb{R}$ and, without loss of generality, that the origin is the nominal equilibrium point of each mode, that is, $f_i(0) = 0$ for all $i \in \mathfrak{I}$. We also assume that the state x does not jump at the switching instants, that is, the solution $x(\cdot)$ is everywhere continuous. Note that changes in the discrete state $\sigma(t)$ (that is, transitions between the continuous dynamical modes) may, in general, be a function of time, state, or both. When changes in $\sigma(t)$ depend only on inherent process characteristics, the switching is referred to as autonomous. However, when $\sigma(t)$ is chosen by some higher process such as a controller or human operator, the switching is referred to as controlled. In this article, we focus on controlled switching where mode transitions are decided and executed by some higher-level supervisor. This class of systems arises naturally in the context of coordinated supervisory and feedback control of chemical-process systems (see the illustrative example below and the simulation studies toward the end of this article).

Finally, we recall the definition of a robust control Lyapunov function that will be used in the development of the main results of this article.

Definition 1 (Freeman and Kokotovic, 1996). A smooth, proper, and positive definite function $V: \mathbb{R}^n \to \mathbb{R}_+$ is called a robust control Lyapunov function for a system of the form $\dot{x} = f(x) + G(x)u + W(x)\theta$ when there exist a function, $\alpha_v(\cdot)$, of class $\mathcal{K}$, and $c_v > 0$ such that

$$\inf_{u \in \mathfrak{U}} \sup_{\theta \in \Theta} \left[L_f V(x) + L_G V(x) u + L_W V(x) \theta + \alpha_v(x) \right] < 0 \tag{2}$$

whenever $V(x) > c_v$, where $L_f V(x) = (\partial V/\partial x) f(x)$, $L_G V(x)$ and $L_W V(x)$ are row vectors of the form $[L_{g_1} V(x) \cdots L_{g_m} V(x)]$, and $[L_{w_1} V(x) \cdots L_{w_q} V(x)]$, respectively, with g_k and w_k referring to the kth columns of the matrices G and W, respectively.

For several classes of nonlinear systems of practical interest, systematic methods are available for the construction of Lyapunov functions that can be used as control Lyapunov functions (see the discussion on feedback linearizable processes, following Remark 11, and the examples in the simulation studies).

Stability Analysis of Hybrid Processes via Multiple Lyapunov Functions

For purely continuous-time nonlinear processes, Lyapunov techniques provide useful tools for stability analysis as well as nonlinear and robust controller design (for example, see El-Farra and Christofides, 2001b, 2003). The basic conceptual idea behind any Lyapunov design is that of "energy shaping," where an appropriate "energy" function (called a Lyapunov function) is chosen for the system, and the controller is designed in a way that enforces the monotonic decay of this function along the trajectories of the closed-loop system (energy dissipation). Given the view of hybrid processes as a finite collection of continuous-time nonlinear processes with discrete events that govern the transition between them, it is quite intuitive to exploit Lyapunov tools to analyze stability of hybrid processes. In this direction, one of the main tools for analyzing stability is MLF (see, for example, DeCarlo et al., 2000). The MLF framework extends, in many respects, the classic energy-shaping idea of Lyapunov analysis for con-

tinuous-time systems to switched systems, but provides, in addition, the tools necessary to account for the hybrid dynamics of such systems. Preparatory for its use later in robust control, we will briefly review in this section the main idea of MLF analysis. To this end, consider the switched process of Eq. 1, with $u_i = \theta_i \equiv 0$, $i = 1, \cdots, N$, and suppose that we can find a family of Lyapunov functions $\{V_i : i \in \mathfrak{I}\}$ such that the value of V_i decreases on each interval when the ith subsystem is active, that is

$$V_i\big(x(t_{i'_k})\big) < V_i\big(x(t_{i_k})\big) \tag{3}$$

for all $i \in \mathfrak{I}$, $k \in Z_+$. The key idea here is that, even if there exists such a Lyapunov function for each subsystem, f_i, individually (that is, each mode is stable), restrictions must be placed on the switching logic to guarantee stability of the overall switched system. The reason is that during the time periods when a particular mode is inactive, its energy might be adversely affected by the evolution of the active mode, such that, the next time that the inactive mode is activated, its energy already exceeds the level it had attained during its last period of activity. When this happens, the overall energy of the system can keep increasing indefinitely, as the process keeps switching in and out between the various modes, thus leading to instability. In fact, it is easy to construct examples of globally asymptotically stable systems and a switching rule that sends all trajectories to infinity [see Branicky (1998), for some classic examples]. There are multiple ways of guarding against such instability due to switching. One possibility is to require, in addition to Eq. 3, that for every $i \in \mathfrak{I}$, the value of V_i at the beginning of each interval on which the ith mode is active exceed (or be, at least, equal to) the value at the beginning of the next such interval (see Figure 2); more precisely

$$V_{\sigma(t_{i_{k+1}})}\big[x(t_{i_{k+1}})\big] \le V_{\sigma(t_{i_k})}\big[x(t_{i_k})\big] \tag{4}$$

where $\sigma(t_{i_{k+1}}) = \sigma(t_{i_k}) = i$. This guarantees that the switched system is Lyapunov stable [see DeCarlo et al. (2000) and the references therein for alternative switching rules]. In Theorem 1 below, a stronger switching condition than the one given in Eq. 4 will be invoked to enforce asymptotic stability in the overall switched closed-loop system (that is, to enforce both Lyapunov stability and asymptotic convergence to the origin).

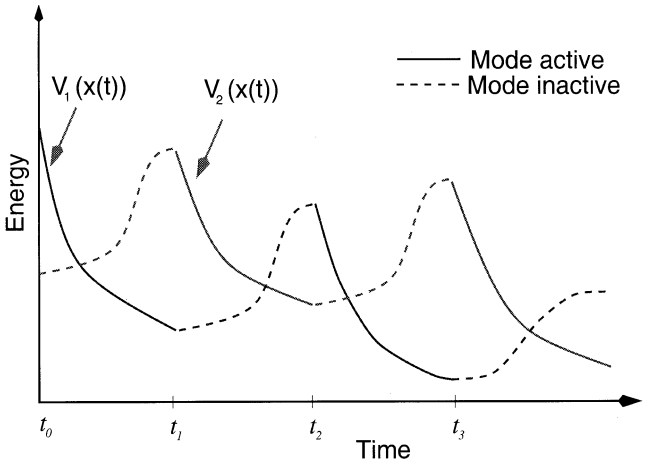

Figure 2. Temporal evolution of multiple Lyapunov functions for an asymptotically stable, two-mode switched system.

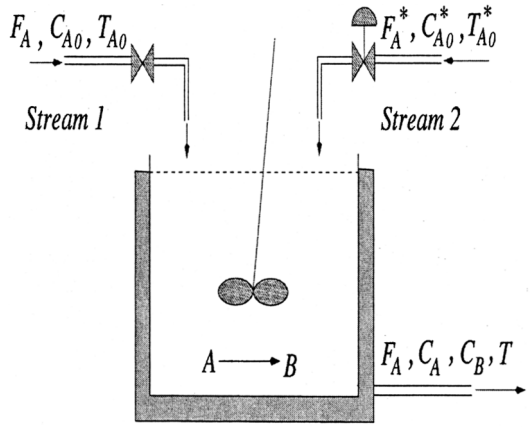

Figure 3. Switched nonisothermal continuous stirred-tank reactor.

Illustrative example: A switched nonisothermal chemical reactor

In this section, we introduce an example of a hybrid nonlinear chemical process with model uncertainty and actuator constraints that will be used throughout the article to illustrate the implementation of the hybrid control strategy. To this end, consider a continuous stirred-tank reactor where an irreversible first-order exothermic reaction of the form $A \xrightarrow{k} B$ takes place. As shown in Figure 3, the reactor has two inlet streams: the first continuously feeds pure A at flow rate F, concentration C_{A0}, and temperature T_{A0}, while the second has a control valve that can be turned on or off depending on operational requirements. When the control valve is open, the second stream feeds pure A at flow rate F^*, concentration C^*_{A0} and temperature T^*_{A0}. Under standard modeling assumptions, the mathematical model for the process takes the form

$$\begin{aligned} V\frac{dC_A}{dt} &= F(C_{A0} - C_A) + \sigma(t)F^*(C^*_{A0} - C_A) \\ &\quad - k_0 \exp\left(\frac{-E}{RT}\right)C_A V \\ V\frac{dT}{dt} &= F(T_{A0} - T) + \sigma(t)F^*(T^*_{A0} - T) \\ &\quad + \frac{(-\Delta H_r)}{\rho c_p}k_0 \exp\frac{-E}{RT}C_A V + \frac{Q}{\rho c_p} \end{aligned} \tag{5}$$

where C_A denotes the concentration of A, T denotes the reactor temperature; Q denotes the rate of heat input/removal from the reactor; V denotes the reactor volume; k_0, E, ΔH denote the preexponential constant, the activation energy, and the enthalpy of the reaction; c_p and ρ denote the heat capacity and density of the fluid in the reactor. The process parameters and steady-state values are given in Table 1.

Table 1. Process Parameters and Steady-State Values for the Chemical Reactor of Eq. 5

$V = 0.1$	m^3
$R = 8.314$	kJ/kmol·K
$C_{A0} = 1.0$	kmol/m^3
$T_{A0s} = 310.0$	K
$\Delta H_{nom} = -400$	kJ/kmol
$k_0 = 2.0 \times 10^7$	s^{-1}
$E = 8.314 \times 10^4$	kJ/kmol
$c_p = 0.002$	kJ/kg·K
$\rho = 1000.0$	kg/m^3
$F = 2.77 \times 10^{-5}$	m^3/s
$C_{As}(\sigma = 0) = 0.577$	kmol/m^3
$T_s(\sigma = 0) = 395.3$	K
$F^* = 5.56 \times 10^{-5}$	m^3/s
$C_{A0}^* = 2.0$	kmol/m^3
$T_{A0S}^* = 350.0$	K

The discrete control variable $\sigma(t)$ takes a value of zero when the control valve is closed and a value of one when the valve is open. Initially, we assume that the valve is closed (that is, $\sigma(0) = 0$). During reactor operation, however, it is desired to open this valve and feed additional reactant material through the second inlet stream (that is, $\sigma = 1$) in order to enhance the product concentration leaving the reactor.

This requirement gives rise to two distinct modes of reactor operation, between which switching is desired. These modes correspond to the off ($\sigma = 0$)/on ($\sigma = 1$) conditions of the control valve on the second inlet stream. Since the initial operating mode ($\sigma = 0$) has an open-loop unstable steady-state that corresponds to $T_s = 395.3$ K, our control objective will be to stabilize the reactor temperature at this point by manipulating the rate of heat input. However, since switching to the second mode ($\sigma = 1$) at some later point in time can potentially destabilize the process, our switching objective will be to carry out the transition between the two modes at the earliest time that does not jeopardize process stability. The control and switching objectives are to be accomplished in the presence of (1) hard constraints on the manipulated input, $|Q| \le 80$ KJ/h, (2) time-varying external disturbances in the feed temperature of both inlet streams, and (3) time-varying parametric uncertainty in the enthalpy of reaction. Note that the disturbances in the feed temperature of the second inlet stream take effect only after switching and, therefore, impact only the second mode, while the disturbances in the first stream's temperature and the parametric uncertainty in the enthalpy influence both modes.

Coordinating Feedback and Switching for Robust Hybrid Control

Problem formulation and solution overview

Consider the switched nonlinear process of Eq. 1 where, for each $i \in \mathfrak{I}$, a robust control Lyapunov function, V_i, is available, the vector of manipulated inputs, u_i, is constrained by $\|u_i\| \le u_i^{\max}$, and the vector of uncertain variables is bounded by $\|\theta_i\| \le \theta_{bi}$, where the notation $\|\cdot\|$ denotes the Euclidean norm of a vector. The bounds that capture the size of the uncertainty can be arbitrarily large. Two control problems will be considered. In the first problem, the uncertain variables are assumed to be vanishing, in the sense that $W_i(0)\theta_i = 0$ for any $\theta_i \in \Theta$ (note that this does not require the variable θ_i itself to vanish in time). Under this assumption, the origin, which is an equilibrium point for the nominal modes of the hybrid process, is an equilibrium point for the uncertain modes as well. For this case, and given that switching is controlled by a higher-level supervisor, the problem is how to coordinate switching between the constituent modes and their respective controllers in a way that respects the constraints and guarantees asymptotic stability of the overall closed-loop system in the presence of uncertainty. To address the problem, we formulate the following objectives. The first is to synthesize, using a family of Lyapunov functions, a family of N bounded robust nonlinear continuous feedback-control laws of the general form

$$u_i = -k_i(V_i, u_i^{\max}, \theta_{bi})(L_{G_i}V_i)^T, \qquad i = 1, \ldots, N \quad (6)$$

which (1) enforce robust asymptotic stability, for their respective closed-loop subsystems, and (2) provide, for each mode, an explicit characterization of the set of admissible initial conditions starting from where a given mode is guaranteed to be stable in the presence of model uncertainty and input constraints. The scalar gain, $k_i(\cdot)$, of the L_GV controller in Eq. 6 is to be designed so that $\|u_i\| \le u_i^{\max}$ and the energy of the ith mode, as captured by V_i, is monotonically decreasing whenever that mode is active. The second objective is to construct a set of robust switching laws that supply the supervisor with the set of switching times that guarantee stability of the constrained uncertain switched closed-loop system, which in turn determines the time course of the discrete state $\sigma(t)$.

In the second control problem, the uncertain variables are assumed to be nonvanishing, in the sense that $W_i(0)\theta_i \neq 0$ for all $i \in \mathfrak{I}$. In this case, the origin is no longer an equilibrium point of the uncertain modes or the overall hybrid process, and, therefore, the objective is to coordinate feedback-controller synthesis and switching in a way that guarantees boundedness of the states of the hybrid process, with an arbitrary degree of attenuation of the effect of uncertainty.

Having formulated the preceding robust hybrid control problems, we proceed in the following two subsections to present their solutions. The first result, given in Theorem 1 below, addresses the problem of vanishing uncertainty, while the second result, given in Theorem 2, deals with the problem of nonvanishing uncertainty.

Hybrid control strategy under vanishing uncertainty

Theorem 1 below summarizes the proposed robust hybrid control strategy for the case when the uncertainty does not affect the nominal equilibrium point of the hybrid process. Provided in this theorem are the formulas of the family of continuous bounded robust feedback controllers, together with the appropriate switching rules used by the supervisor to govern the transitions between the various closed-loop modes in a way that guarantees the desired properties in the constrained uncertain hybrid closed-loop system. The proof of this theorem is given in Appendix A.

Theorem 1. Consider the switched uncertain nonlinear process of Eq. 1, where $W_i(0)\theta_i = 0$ for all $i \in \mathfrak{I}$, under the following family of bounded nonlinear feedback controllers

$$u_i = -k_i(V_i, u_i^{\max}, \theta_{bi}, \chi_i, \phi_i)(L_{G_i}V_i)^T, \qquad i = 1, \ldots, N \quad (7)$$

where

$$k_i(\cdot)=\begin{cases}\dfrac{L_{f_i}^{*}V_i+\sqrt{\left(L_{f_i}^{**}V_i\right)^2+\left(u_i^{\max}\,\|\left(L_{G_i}V_i\right)^T\|\right)^4}}{\left(\|\left(L_{G_i}V_i\right)^T\|\right)^2\left[1+\sqrt{1+\left(u_i^{\max}\,\|\left(L_{G_i}V_i\right)^T\|\right)^2}\right]}, & \|\left(L_{G_i}V_i\right)^T\|\neq 0\\ 0 & \|\left(L_{G_i}V_i\right)^T\|=0\end{cases} \tag{8}$$

$$L_{f_i}^{*}V_i=L_{f_i}V_i+\left(\rho_i\|x\|+\chi_i\|\left(L_{W_i}V_i\right)^T\|\theta_{bi}\right)\left(\frac{\|x\|}{\|x\|+\phi_i}\right)$$

$$L_{f_i}^{**}V_i=L_{f_i}V_i+\rho_i\|x\|+\chi_i\|\left(L_{W_i}V_i\right)^T\|\theta_{bi} \tag{9}$$

V_i is a robust control Lyapunov function for the ith subsystem and ρ_i, χ_i, ϕ_i are tunable parameters that satisfy $\rho_i>0, \chi_i>1$ and $\phi_i>0$. Let $\Omega_i^{*}(u_i^{\max},\theta_{bi})$ be the largest invariant set embedded within the region described by the inequality

$$L_{f_i}V_i+\rho_i\|x\|+\chi_i\|\left(L_{W_i}V_i\right)^T\|\theta_{bi}\le u_i^{\max}\|\left(L_{G_i}V_i\right)^T\| \tag{10}$$

and assume, without loss of generality, that $x(0)=x_0\in\Omega_i^{*}(u_i^{\max},\theta_{bi})$ for some $i\in\mathfrak{I}$. If, at any given time T such that

$$x(T)\in\Omega_j^{*}\left(u_j^{\max},\theta_{bj}\right) \tag{11}$$

$$V_j(x(T))<V_j\left(x\left(t_{j'}\right)\right) \tag{12}$$

for some $j\in\mathfrak{I}$, $j\neq i$, where $t_{j'}$ is the time when the jth subsystem was last switched out, that is, $\sigma(t_{j'}^{+})\neq\sigma(t_{j'}^{-})=j$, we set $\sigma(T^{+})=j$, then there exists a positive real number ϕ_j^{*} such that for any $\phi_j\le\phi_j^{*}$, the origin of the switched closed-loop system is asymptotically stable.

Remark 1. The bounded robust feedback controllers given in Eqs. 7–9 are synthesized, using MLFs, by reshaping the scalar nonlinear gain of the L_GV controller proposed originally in Lin and Sontag (1991) [see also El-Farra and Christofides (2003)], in order to account for the effect of the uncertain variables. As a result, the control action now depends explicitly on both the magnitude of the input constraints, $u_i^{\max}$, and the size of the uncertainty, θ_{bi}. Note that the only information about the size of the uncertainty (and not the uncertainty itself) is needed for controller design and that this size can be arbitrarily large. Each controller in Eqs. 7–9 is a smooth function of the state away from the origin. It is also continuous at the origin whenever the corresponding control Lyapunov function satisfies the small control property [see Lin and Sontag (1991) for details].

Remark 2. Each controller in Eqs. 7–9 possesses two tuning parameters, ϕ_i and χ_i, responsible for enforcing robust stability and achieving the desired degree of attenuation of the effect of uncertainty on each of the constituent modes of the hybrid process. A significant degree of attenuation can be achieved by selecting the parameter ϕ_i to be sufficiently small and/or choosing the parameter χ_i to be sufficiently large (see step 1 in the proof of Theorem 1). Another important feature of the uncertainty compensator (that is, the term $\chi_i\|(L_{W_i}V_i)^T\|\theta_{bi}$) used in designing the controller gain of Eqs. 8–9 is the presence of a scaling function, of the form $\|x\|/(\|x\|+\phi_i)$, which multiplies the compensator. Since ϕ_i is a small positive number, the scaling function approaches a value of 1 when $\|x\|$ is large (far from the equilibrium point) and a value of zero when $\|x\|$ is small (close to the equilibrium point). This allows us, as we get closer to the equilibrium point, to use smaller control effort to cancel the uncertainties. The full weight (or gain) of the uncertainty compensator is used only when the state is far from the equilibrium point.

Remark 3. The use of bounded nonlinear controllers of the form of Eqs. 7–9 to robustly stabilize the constituent modes is motivated by the fact that this class of controllers provides an explicit characterization of the limitations imposed by uncertainty and constraints on the region of closed-loop stability. Specifically, each controller in Eqs. 7–9 provides an explicit characterization of the set of admissible initial conditions, starting from where robust closed-loop stability of the corresponding subsystem is guaranteed with the available control action. This characterization can be obtained from the set of inequalities given in Eq. 10. For each mode, the corresponding inequality describes a closed region in the state space [henceforth denoted by $\Phi_i(u_i^{\max},\theta_{bi})$] where the corresponding control law satisfies the constraints and the associated Lyapunov function, V_i, decreases monotonically (see step 1 in the proof of Theorem 1). Owing to the presence of uncertainty, the size of Φ_i now depends on the size of the uncertainty, in addition to the magnitude of input constraints. The larger the uncertainty and/or the tighter the constraints, the smaller Φ_i is in size. It is important to note that even though a trajectory starting in Φ_i will move from one Lyapunov surface to an inner Lyapunov surface with lower energy (because $\dot{V}_i<0$) there is no guarantee that the trajectory will remain forever in Φ_i, since it is not necessarily a region of invariance. Once the trajectory leaves Φ_i, however, there is no guarantee that $\dot{V}_i<0$. To guarantee that $\dot{V}_i$ remains negative for all times during which the ith mode is active, we compute the largest invariant set $\Omega_i^{*}(u_i^{\max},\theta_{bi})$ within $\Phi_i(u_i^{\max},\theta_{bi})$ [see Khalil (1996) for details on how to construct these sets]. This set, which is also parameterized by the constraints and the uncertainty bounds, represents an estimate of the stability region associated with each mode. Finally, note that in the absence of any plant–model mismatch, that is, $\theta_{bi}\equiv 0$, the controllers of Eqs. 7–9, together with the expressions for the stability regions, Ω_i^{*}, reduce to those de-

veloped in El-Farra and Christofides (2002) under nominal conditions.

Remark 4. Each of the inequalities in Eq. 10 captures the trade-off between the size of the stability region and the degree of uncertainty attenuation. To see this, note that the size of the region of guaranteed closed-loop stability, obtained from Eq. 10, can be enlarged by using small values for the controller tuning parameters, χ_i and ρ_i. This enlargement of the stability region, however, comes at the expense of the controller's robust performance, since large values for χ_i and ρ_i are typically required to achieve a significant degree of attenuation of the effect of disturbances and plant–model mismatch on the closed-loop system. Therefore, in selecting the controller tuning parameters, one must strike a balance between the need to stabilize the process from a given initial condition and the requirement of achieving a satisfactory degree of uncertainty attenuation.

Remark 5. The two switching laws of Eqs. 11–12 determine, implicitly, the time(s) when switching from mode i to mode j is permissible. The first rule tracks the temporal evolution of the continuous state, x, and requires that, at the desired time for switching, the continuous state be within the stability region of the target mode, $\Omega_j^*(u_j^{\max}, \theta_{bj})$. A pictorial representation of this idea is shown in Figure 4. This requirement ensures that, once the target mode and its corresponding controller are engaged, the corresponding Lyapunov function continues to decay for as long as the mode remains active. Note that this condition must be enforced every time that the supervisor considers switching between modes. In contrast, the second switching rule of Eq. 12 is checked only if the target mode has been activated (at least once) in the past. In this case, Eq. 12 allows reactivation of mode j provided that its energy at the current "switch in" is less than its energy at the last "switch out." This condition guarantees that, whenever a given mode is activated, the closed-loop state is closer to the origin than it was when the same mode was last activated. Note that if each of the N modes is activated only once during the course of operation (that is, we never switch back to a mode previously activated), the second condition is automatically satisfied. Furthermore, for the case when only a finite number of switches (over the infinite time interval) is considered, this condition can be relaxed by allowing switching to take place even when the value of V_j, at the desired switching time, is larger than that when mode j was last switched in, as long as the increase is finite. The reason is that these finite increases in V_j (resulting from switching back to mode j) will be overcome when the process eventually settles in the "final" mode, whose controller, in turn, forces its Lyapunov function to continue to decay as time tends to infinity, thus asymptotically stabilizing the overall hybrid process.

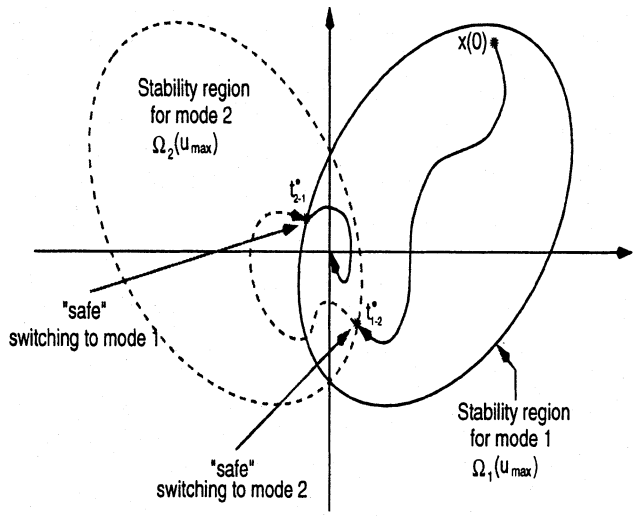

Figure 4. Implementation of the switching law based on monitoring the evolution of the closed-loop trajectory with respect to stability regions.

Remark 6. It is important to note that the switching scheme proposed in Theorem 1 is only sufficient to guarantee closed-loop stability. If the conditions in Eqs. 11–12 are satisfied at a given time instance, then we conclude that it is "safe" to switch from the current mode/controller combination to the one for which the conditions hold. However, it is not necessary to switch at this time to maintain closed-loop stability. The reason is the fact that the initial condition belongs to the closed-loop stability region of at least one of the constituent modes. Therefore, even if switching does not take place, the closed-loop trajectory will remain in this set and stabilize at the desired equilibrium point. In many practical situations, however, changes in operational conditions and requirements typically motivate switching between various process modes. Also, in cases of control system failures, switching between multiple control configurations is typically necessary to preserve closed-loop stability. In all of these cases, the result of Theorem 1 provides a strategy for carrying out mode transitions without jeopardizing the stability of the overall process (see the simulation studies below for examples).

Remark 7. Note that it is possible for more than one subsystem, j, to satisfy the switching rules given in Eqs. 11–12. This occurs when the process state lies within the intersection of several stability regions. In this case, Theorem 1 guarantees only that a transition from the current mode to any of these modes is safe, but does not suggest which one to choose, since they all guarantee stability. The decision to choose a particular mode to activate is typically made by the supervisor based on the particular operational requirements of the process.

Remark 8. Referring to the practical applications of Theorem 1, one must initially identify the constituent modes of the hybrid process. A Lyapunov function is then constructed for each mode to synthesize, via Eqs. 7–9, a bounded robust controller and construct, with the aid of Eq. 10, the region of closed-loop stability associated with each mode. Implementation of the control strategy then proceeds by initializing the process within the stability region of the desired initial mode of operation and implementing the corresponding robust controller. Then, the switching the laws of Eqs. 11–12 are checked on-line by the supervisor to determine if it is possible to switch the operation mode to a particular mode at some time. If the conditions are satisfied, then a transition to that mode (and its controller) is executed. If the conditions are not satisfied, then the current operating mode is kept active. A summary of the proposed robust hybrid control methodology is shown in Figure 5.

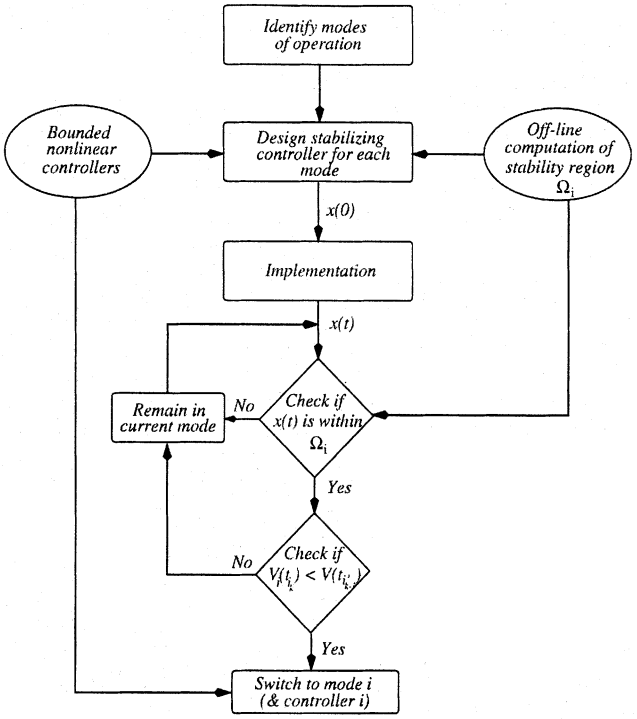

Figure 5. Hybrid control strategy based on coordinating feedback and switching.

Hybrid control strategy under nonvanishing uncertainty

In this section, we address the problem of nonvanishing uncertainty, where the uncertainty changes the nominal equilibrium point of the hybrid process. Theorem 2 below summarizes the proposed hybrid control strategy for this case and states, precisely, the resulting closed-loop properties. The proof of this theorem is given in Appendix B.

Theorem 2. Consider the switched uncertain nonlinear process of Eq. 1, where $W_i(0)\theta_i \neq 0$ for all $i \in \mathfrak{I}$, under the family of controllers given in Eqs. 7–9. Assume, without loss of generality, that $x(0) \in \Omega_i^*(u_i^{\max}, \theta_{bi})$ for some $i \in \mathfrak{I}$ and that, for any given $T > 0$, $\sigma(T^+) = j$ only if the conditions of Eqs. 11–12 hold for some $j \in \mathfrak{I}$, $j \neq i$. Then, given any arbitrarily small real number $d > 0$, there exist a set of positive real numbers $\{\epsilon_1^*, \ldots, \epsilon_N^*\}$ such that if $\epsilon_i \leq \epsilon_i^*$, for all $i \in \mathfrak{I}$, the trajectories of the switched closed-loop system are bounded and satisfy $\limsup_{t \to \infty} \| x(t) \| \leq d$, where $\epsilon_i = \phi_i / (\chi_i - 1)$.

Remark 9. Owing to the nonvanishing nature of the uncertainty influencing each mode, asymptotic convergence to the origin is not possible, via continuous feedback, for any of the constituent modes of the hybrid process. However, in lieu of asymptotic stability, one can show (see the proof of Theorem 2 in Appendix B) that, for every mode i by itself (without switching), the corresponding controller guarantees convergence of the closed-loop trajectory, in finite time, to a small neighborhood of the origin (called a residual or terminal set) such that the trajectory, once inside this set, cannot escape [see El-Farra and Christofides (2001b, 2003) for further details]. The size of this set can be made arbitrarily small by choosing the controller tuning parameter ϕ_i to be sufficiently small and/or selecting the tuning parameter χ_i to be sufficiently large. In this manner, one can achieve an arbitrary degree of robust attenuation of the effect of uncertainty on each mode of the closed-loop system.

Remark 10. Boundedness of the state of the constituent modes does not, by itself, imply boundedness of the state of the overall hybrid process. Boundedness of the switched closed-loop trajectory can be ensured using the switching rules given in Eqs. 11–12, which automatically impose constraints on which a mode can be engaged at any given time. These constraints, similar to the case of the vanishing uncertainty, guarantee that, whenever a mode is activated (or reactivated), not only is its energy less than what it was before (Eq. 12), but also this energy continues to decay for as long as the mode remains active (Eq. 11). The only difference in the case of nonvanishing uncertainty is that these rules need only be implemented by the supervisor when the state lies outside the residual set. To understand the rationale for this observation, we first observe that, since the size of the residual set of each mode can be tuned (by appropriately adjusting ϕ_i and χ_i), a small common residual set that is completely contained within the intersection of the various stability regions can be chosen for all the modes. Then, starting from any admissible initial condition, implementation of the switching logic outside this residual set ensures that, for every mode, the closed-loop trajectory moves closer and closer to that set as we switch in and out of that mode. Since the number of process modes is finite, and only a finite number of switches is allowed over any finite time interval, then at least one of the constituent modes will converge, in finite time, to the residual set. From that time onward, the closed-loop trajectory stays within the common residual set for all times, regardless of any further mode switchings (see step 2 in the proof of Theorem 2 for the mathematical details).

Remark 11. Theorems 1 and 2 consider, respectively, the cases when the uncertainties affecting the various modes are either all vanishing or all nonvanishing. For the general case when the uncertainty is vanishing for some modes and nonvanishing for others, one can establish only boundedness of the closed-loop trajectory. If, however, only a finite number of switches is allowed over the infinite time interval, then one can establish asymptotic stability if the uncertainty, influencing the final mode where the hybrid process eventually settles, is vanishing. If such uncertainty, on the other hand, is nonvanishing, then the closed-loop trajectory will instead reach and enter, in finite time, the residual set of the final mode without ever leaving again.

Application to input/output linearizable processes with uncertainty

An important class of nonlinear processes that has been studied extensively within process control is that of input/output feedback linearizable processes. This class arises frequently in practical problems where the objective is to force the controlled output to follow some reference-input trajectory (rather than stabilize the full state at some nominal equilibrium point). In this section, we illustrate how the coordinated robust feedback and switching methodology proposed in the previous section can be applied when the individual modes of the hybrid process are input/output linearizable. For simplicity, we limit our attention to the single-input sin-

gle-output case with vanishing uncertainty. Consider the hybrid process

$$\begin{aligned}\dot{x}(t) &= f_{\sigma(t)}[x(t)] + g_{\sigma(t)}[x(t)]u_{\sigma(t)} + w_{\sigma(t)}[x(t)]\theta_{\sigma(t)}\\ y &= h(x)\\ \sigma(t) &\in \mathfrak{I} = \{1, \ldots, N\}\end{aligned} \tag{13}$$

where $y \in \mathbb{R}$ is the controlled output and $h(x)$ is a sufficiently smooth scalar function. Suppose that, for all $i \in \mathfrak{I}$, there exists an integer r (this assumption is made only to simplify notation and can be readily relaxed to allow a different relative degree r_i for each mode) and a set of coordinates (see Isidori (1995) for a detailed treatment of feedback linearizable nonlinear systems)

$$\begin{bmatrix}\zeta\\ \eta\end{bmatrix} = \begin{bmatrix}\zeta_1\\ \zeta_2\\ \vdots\\ \zeta_r\\ \eta_1\\ \vdots\\ \eta_{n-r}\end{bmatrix} = \chi(x) = \begin{bmatrix}h(x)\\ L_{f_i}h(x)\\ \vdots\\ L_{f_i}^{r-1}h(x)\\ T_{1,i}(x)\\ \vdots\\ T_{n-r,i}(x)\end{bmatrix} \tag{14}$$

where $T_1(x), \ldots, T_{n-r}(x)$ are nonlinear scalar functions of x, such that the system of Eq. 13 takes the form

$$\begin{aligned}\dot{\zeta}_1 &= \zeta_2\\ &\vdots\\ \dot{\zeta}_{r-1} &= \zeta_r\\ \dot{\zeta}_r &= L_{f_i}^r h\left[\chi^{-1}(\zeta,\eta)\right] + L_{g_i}L_{f_i}^{r-1}h\left[\chi^{-1}(\zeta,\eta)\right]u_i\\ &+ L_{w_i}L_{f_i}^{r-1}h\left[\chi^{-1}(\zeta,\eta)\right]\theta_i\\ \dot{\eta}_1 &= \Psi_{1,i}(\zeta,\eta)\\ &\vdots\\ \dot{\eta}_{n-r} &= \Psi_{n-r,i}(\zeta,\eta)\\ y &= \zeta_1\end{aligned} \tag{15}$$

where $L_{g_i}L_{fi}^{r-1}h(x) \neq 0$ for all $x \in \mathbb{R}^n$, $i \in \mathfrak{I}$. Under the assumption that the η-subsystem is input-to-state stable (ISS) with respect to ζ for each $i \in \mathfrak{I}$ (see Sontag (1989) for the definition of ISS), the controller synthesis task for each mode can be addressed on the basis of the partially linear ζ-subsystem. To this end, upon introducing the notation $e_k = \zeta_k - \upsilon^{(k-1)}$, $e = [e_1 e_2 \cdots e_r]^T$, $\bar{\upsilon} = [\upsilon\, \upsilon^{(1)} \cdots \upsilon^{(r-1)}]T$, where $\upsilon^{(k)}$ is the kth time derivative of the reference input υ, which is assumed to be a smooth function of time, the ζ-subsystem of Eq. 15 can be further transformed into the following more compact form

$$\dot{e} = \bar{f}_i(e,\eta,\bar{\upsilon}) + \bar{g}_i(e,\eta,\bar{\upsilon})u_i + \bar{w}_i(e,\eta,\bar{\upsilon})\theta_i, \qquad i = 1, \ldots, N \tag{16}$$

where $\bar{f}_i(e,\eta,\bar{\upsilon}) = Ae + bL_{f_i}^r h(\chi^{-1}(e,\eta,\bar{\upsilon}))$ and $\bar{g}_i(e,\eta,\bar{\upsilon}) = bL_{g_i}L_{fi}^{r-1}h(\chi^{-1}(e,\eta,\bar{\upsilon}))$, $\bar{w}_i(e,\eta,\bar{\upsilon}) = bL_{w_i}L_{f_i}^{r-1}h(\chi^{-1}(e,\eta,\bar{\upsilon}))$ are $r \times 1$ vector functions, and

$$A = \begin{bmatrix}0 & 1 & 0 & \ldots & 0\\ 0 & 0 & 1 & \ldots & 0\\ \vdots & & & & \vdots\\ 0 & 0 & 0 & \ldots & 1\\ 0 & 0 & 0 & \ldots & 0\end{bmatrix}, \qquad b = \begin{bmatrix}0\\ 0\\ \vdots\\ \\ 1\end{bmatrix} \tag{17}$$

are an $r \times r$ matrix and $r \times 1$ vector, respectively. For systems of the form of Eqs. 16–17, a simple choice for a robust control Lyapunov function is a quadratic function of the form $\bar{V}_i = e^T P_i e$, where the positive definite matrix P_i is chosen to satisfy the following Riccati inequality (for example, see Sepulchre et al. (1997))

$$A^T P_i + P_i A - P_i < 0 \tag{18}$$

Using these quadratic functions, a bounded robust controller can be designed for each mode using Eqs. 7–9 applied to the system of Eq. 16–17. Using a standard Lyapunov argument, it can then be shown that each controller robustly asymptotically stabilizes the e states in each mode. This result together with the ISS assumption on the η states can then be used to show, via a small gain argument, that the full closed-loop $e - \eta$ interconnection, for each individual mode, is asymptotically stable.

Remark 12. Note that, since the objective here is output tracking, rather than full state stabilization, the Lyapunov functions used in designing the controllers, $\bar{V}_i$, are in general different from the Lyapunov functions, V_i, used in implementing the switching rules. Owing to the ISS property of the η-subsystem of each mode, only a Lyapunov function for the e-subsystem, namely $\bar{V}_i$, is needed and used to design a controller that robustly stabilizes the full $e - \eta$ interconnection for each mode. However, when implementing the switching rules (constructing the Ω_i^* and verifying Eq. 12), we need to track the evolution of x (and, hence, the evolution of both e and η). Therefore, the Lyapunov functions used in verifying the switching conditions at any given time, V_i, are based on x. From the asymptotic stability of each mode, the existence of these Lyapunov functions is guaranteed by converse Lyapunov theorems [see Chapter 3 in Khalil (1996) for further details]. For systems with relative degree $r = n$, the choice $\bar{V}_i = V_i$ is sufficient.

Simulation Studies

Application to a switched nonisothermal chemical reactor

In this section, we revisit the switched chemical reactor example, introduced earlier in Eq. 5, to illustrate, through computer simulations, the application of the proposed hybrid control strategy. Recall that the control objective is to stabilize the reactor temperature at the open-loop unstable steady state, by manipulating the rate of heat input, while the switching objective is to carry out the transition between the two modes at the earliest time possible without jeopardizing process stability. The control and switching objectives are to be accomplished in the presence of hard constraints on the manipulated input ($|Q| \leq 80$ KJ/h), time-varying external dis-

turbances in the feed temperature of both inlet streams, and time-varying parametric uncertainty in the enthalpy of reaction. For the purpose of simulating the effect of uncertainty on the process output, we consider time-varying functions of the form $\theta(t) = \theta_b \sin(4t)$, where the upper bounds on the feed temperature disturbances are taken to be 10 K for both streams, and the upper bound on the uncertainty in the enthalpy is taken to be 15% of the nominal value. We note that any other bounded and time-varying function can be used to simulate the effect of uncertainty. This choice does not affect the results, since it is only the bounds on these functions that are needed for controller and switching law design.

To accommodate both the control and operational objectives, and since the uncertain variables considered are nonvanishing, we follow the strategy proposed in Theorem 2. For this feedback linearizable process, the controlled output has a relative degree of $r = 1$ and, therefore, using a coordinate transformation of the form of Eq. 14, a scalar system of the form of Eq. 16, describing the input/output dynamics, can be obtained for controller design. Two quadratic positive-definite functions of the form $\overline{V}_i = 0.5 c_i e^2$, where $c_i > 0$ is a constant and $e = T - T_s$, are then used to synthesize, on the basis of the e-subsystems, two bounded nonlinear controllers (one for each mode) and compute their stability regions (note that these functions are CLFs for the e-subsystem only and not for the full system of Eq. 5-see Remark 12). The following tuning parameters were used for each controller: $c_1 = c_2 = 1$; $\phi_1 = \phi_2 = 0.01$; $\chi_1 = 2$, $\chi_2 = 1.1$; $\rho_1 = \rho_2 = 0.001$, to guarantee that the reactor temperature satisfies a relation of the form $\lim_{t \to \infty} \sup |T(t) - T_s| \leq 0.01$.

Several closed-loop simulations were performed to evaluate the proposed control strategy. In the first set of simulation runs, the reactor is operated in the first mode (control valve closed, $\sigma = 0$) for all time, with no switching. The feedback controller designed for this mode is consequently implemented to robustly stabilize the reactor temperature, starting from an admissible initial condition. Figure 6 (solid lines) depicts the resulting reactor temperature (controlled output) and rate of heat input (manipulated input) profiles. Also included in the figure are the corresponding open-loop profiles with no control (dashed lines). We observe that the controller successfully stabilizes the reactor temperature at the desired steady state and simultaneously attenuates the effect of disturbances and model uncertainty on the reactor temperature.

In the second set of simulation runs, we seek to accommodate the operational requirement of increasing the product concentration by switching to the second mode (control valve open, $\sigma = 1$) at some point. Note that switching to the second mode is accompanied by a switch to the second controller responsible for stabilizing this mode. In the absence of any explicit switching guidelines, suppose that the switching time is randomly set to be as early as $t = 12$ min. The resulting temperature and heat input profiles in this case are shown in Figure 7. It is clear from the figure that by switching at this arbitrarily chosen time, the controller for the $\sigma = 1$ mode is unable to stabilize the reactor temperature at the desired steady-state nor attenuate the effect of uncertainty on the reactor temperature. The reason, which is reflected in the input profile, is that at this time, the process state lies outside the stability region of the $\sigma = 1$ mode, and, therefore,

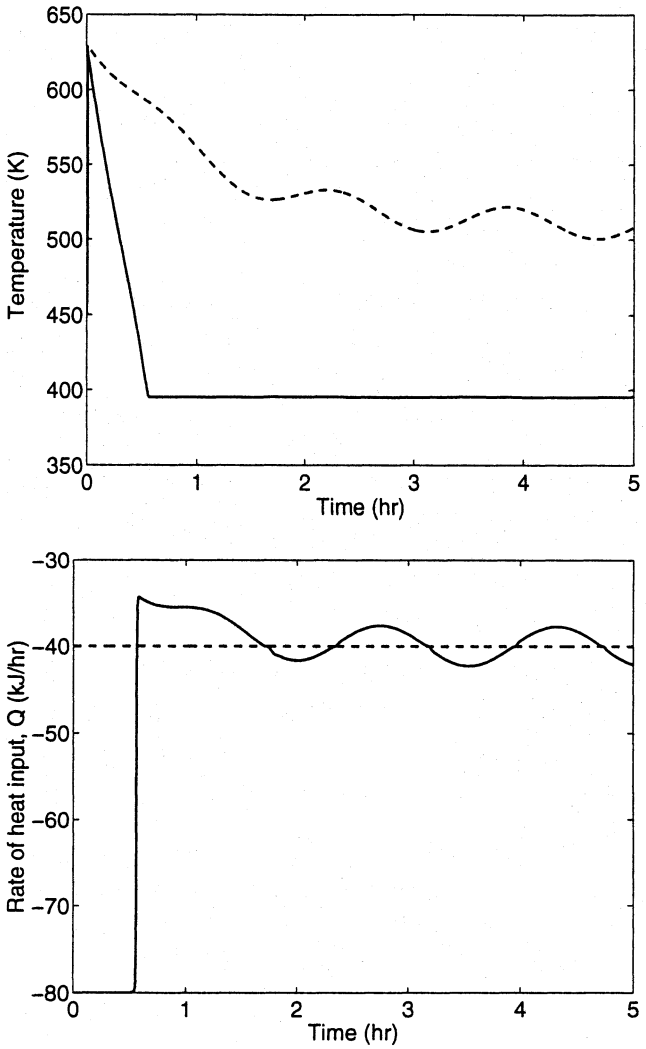

Figure 6. Reactor temperature and rate of heat input profiles under the bounded robust controller of the first mode when the control valve is closed (solid lines) and under open-loop conditions (dashed lines).

the available control action is insufficient to stabilize the temperature.

Now, instead of choosing the switching time arbitrarily, suppose that the nominal switching laws proposed in El-Farra and Christofides (2001a) are used. These laws were used to address a similar switched-reactor control problem under nominal conditions. This case is considered here to study the effect of uncertainty on switching. To this end, consider first the case where no uncertainty is present (that is, $\theta_i \equiv 0$) and initialize the closed-loop system within the first mode (control valve closed, $\sigma = 0$) at the same admissible initial condition, considered previously, using the first controller with $\rho_1 = \chi_1 = 0$. By tracking the closed-loop trajectory in time, it is found that the process state enters the stability region of the second mode at $t = 24$ min. Consequently, the mode transition (including a switch to the second controller with $\rho_2 = \chi_2 = 0$) is carried out at this time. The resulting controlled output and manipulated input profiles are depicted by the solid

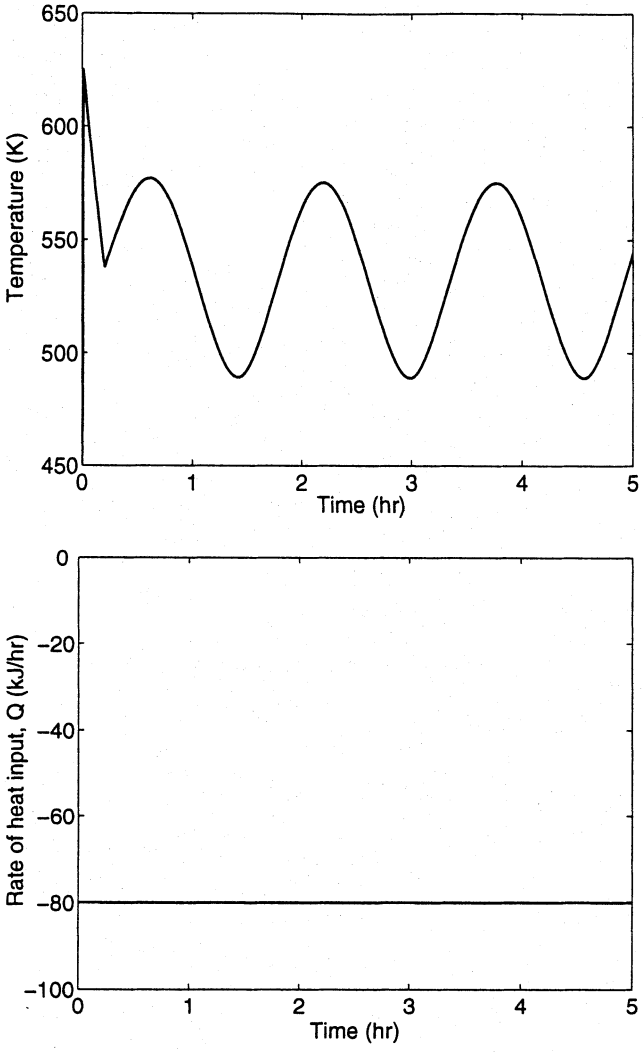

Figure 7. Reactor temperature and rate of heat input profiles when the reactor is initially operated in the first mode (control valve closed, $\sigma = 0$) using the corresponding robust controller, then the control valve is opened ($\sigma = 1$) at $t = 12$ min, and the robust controller for the second mode is activated in place of the first controller.

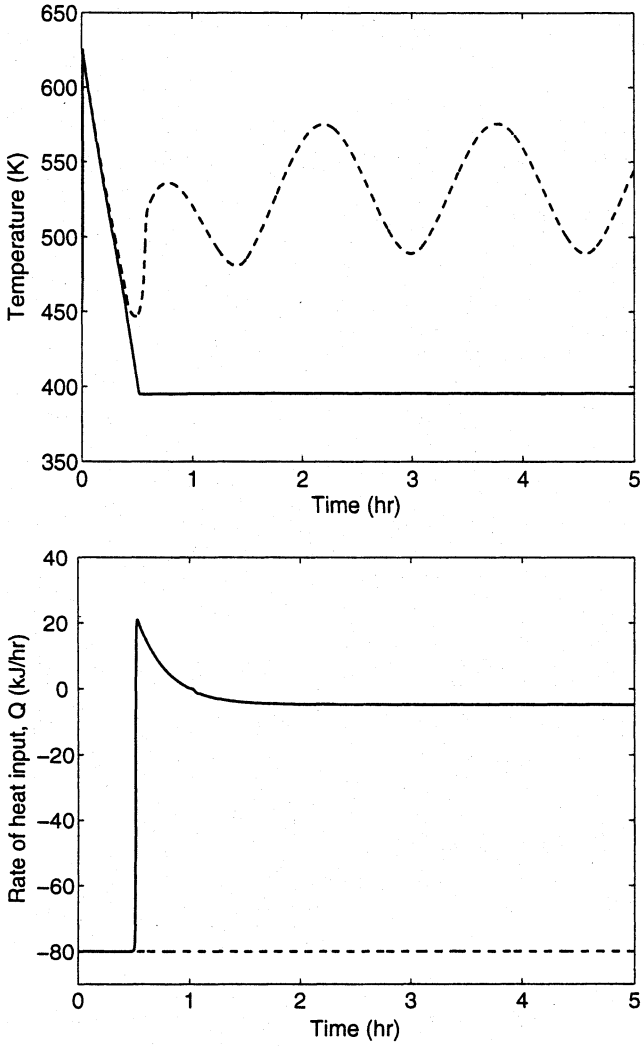

Figure 8. Reactor temperature and rate of heat input profiles for the case when mode switching is carried out at $t = 24$ min with no uncertainty present (solid lines) and for the case when uncertainty is present and mode switching (using nominal controllers with $\rho_i = \chi_i = 0$) is carried out at $t = 24$ min (dashed lines).

lines in Figure 8, which show that the reactor temperature stabilizes at the desired steady state.

Suppose now that the "nominally safe" switching time, $t = 24$ min, is used when model uncertainty is present. The resulting temperature and heat input profiles are shown by the dashed lines in Figures 8 and 9, which depict, respectively, the case when the controllers do not compensate for the effect of uncertainty ($\rho_i = \chi_i = 0$) and the case when they compensate for the effect of uncertainty. It is clear from the unstable behavior in both profiles that the effect of uncertainty is significant and that, even when a robust controller is used in each mode, the nominal switching rules (or times) cannot guarantee closed-loop stability when uncertainty is present. As indicated by the input profiles, which remain saturated for all times, the state lies outside the stability region of the second mode at $t = 24$ min.

In the final set of simulation runs, the switching scheme proposed in Theorem 2, which is based on stability regions that account for the presence of plant–model mismatch, is implemented. In this case, the reactor is initialized in the $\sigma = 0$ mode, using the corresponding robust controller, and then a switch to the $\sigma = 1$ mode (and its robust controller) is carried out only when the condition in Eq. 11 is satisfied (note that the condition of Eq. 12 is not needed, since the initial mode is not reactivated). The controlled output and manipulated input profiles for this case are depicted by the solid lines in Figure 9, which show that the robust hybrid control strategy successfully drives the reactor temperature to the desired steady state while attenuating the effect of uncertainty.

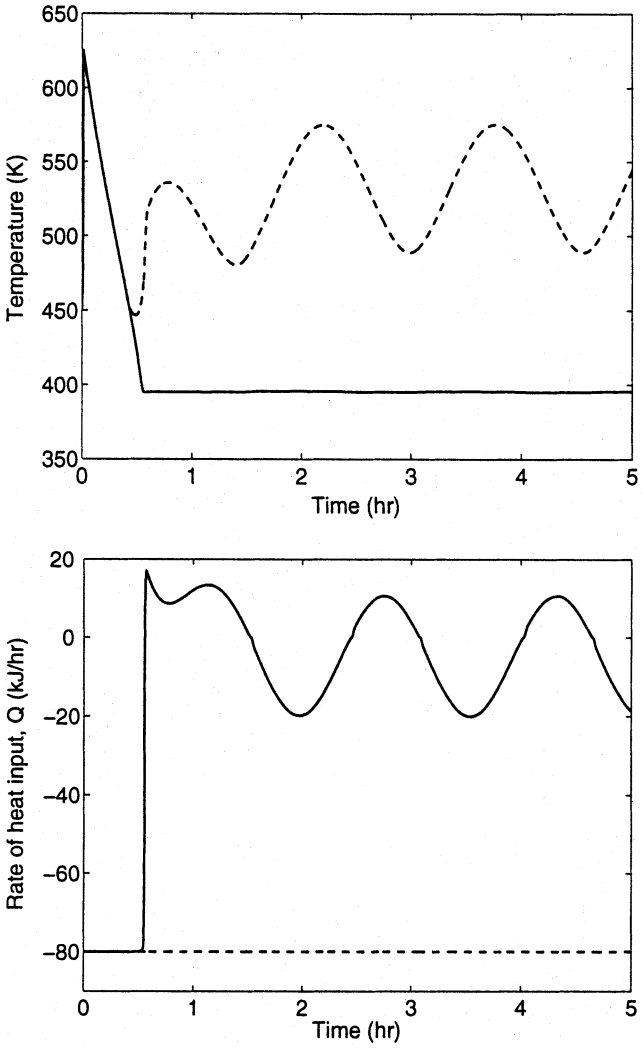

Figure 9. Reactor temperature and rate of heat input profiles for the cases when uncertainty is present and mode switching (using the bounded robust controllers) is carried out at $t = 24$ min (dashed lines) and at $t = 30$ min (solid lines).

The transition between the two modes becomes safe after about 30 min of reactor startup.

Application to fault-tolerant control of a chemical process

Process Description and Problem Formulation. The problem of designing fault-tolerant control systems that can maintain process integrity and stability under the adverse conditions of actuator failure is an important practical problem within process control. The ability of the control system to deal with failure situations typically requires consideration of multiple control configurations and switching between them to preserve closed-loop stability in the event that the active control configuration fails. The occurrence of actuator faults, and the concomitant switching between different control configurations, give rise to hybrid closed-loop dynamics. Our objective in this section is to demonstrate how the hybrid control strategy, proposed in this article, can be used to design and implement fault-tolerant control systems for nonlinear processes with actuator constraints. To this end, consider a well-mixed, nonisothermal continuous stirred-tank reactor where three parallel irreversible elementary exothermic reactions of the form $A \xrightarrow{k_1} B$, $A \xrightarrow{k_2} U$, and $A \xrightarrow{k_3} R$ take place, where A is the reactant species, B is the desired product, and U, R are undesired byproducts. The feed to the reactor consists of pure A at flow rate F, molar concentration C_{A0}, and temperature T_{A0}. Due to the nonisothermal nature of the reactions, a jacket is used to remove/provide heat to the reactor. Under standard modeling assumptions, a mathematical model of the process can be derived from material and energy balances and takes the following form

$$\frac{dT}{dt} = \frac{F}{V}(T_{A0} - T) + \sum_{i=1}^{3} \frac{(-\Delta H_i)}{\rho c_p} k_{i0} e^{-E_i/RT} C_A + \frac{Q}{\rho c_p V}$$

$$\frac{dC_A}{dt} = \frac{F}{V}(C_{A0} - C_A) - \sum_{i=1}^{3} k_{i0} e^{-E_i/RT} C_A$$

$$\frac{dC_B}{dt} = -\frac{F}{V} C_B + k_{10} e^{-E_1/RT} C_A \qquad (19)$$

where C_A and C_B denote the concentrations of the species A and B; T denotes the temperature of the reactor; Q denotes the rate of heat input/removal from the reactor; V denotes the volume of the reactor; ΔH_i, k_i, E_i, $i = 1, 2, 3$, denote the enthalpies, preexponential constants, and activation energies of the three reactions, respectively; and c_p and ρ denote the heat capacity and density of the reactor. The values of the process parameters and the corresponding steady-state values are given in Table 2. It was verified that, under these conditions, the process of Eq. 19 has three equilibrium points (two locally asymptotically stable and one unstable).

The control objective is to stabilize the reactor temperature, reactant, and desired product concentrations at the (open-loop) unstable steady state. To accomplish this objective, in the presence of possible control actuator failures, we consider the following family of manipulated input candidates (see Figure 10):

(1) Rate of heat input, $u_1 = Q$, subject to the constraints $|Q| \le u_1^{\max} = 748$ KJ/s.

Table 2. Process Parameters and Steady-State Values for the Chemical Reactor of Eq. 19

$V = 1.0$	m^3
$R = 8.314$	kJ/kmol·K
$C_{A0} = 4.0$	kmol/m^3
$T_{A0} = 300.0$	K
$\Delta H_1 = -5.0 \times 10^4$	kJ/kmol
$\Delta H_2 = -5.2 \times 10^4$	kJ/kmol
$\Delta H_3 = -5.4 \times 10^4$	kJ/kmol
$k_{01} = 833.3$	s^{-1}
$k_{02} = 83.3$	s^{-1}
$k_{03} = 83.3$	s^{-1}
$E_1 = 5.0 \times 10^4$	kJ/kmol
$E_2 = 7.53 \times 10^4$	kJ/kmol
$E_3 = 7.53 \times 10^4$	kJ/kmol
$c_p = 0.239$	kJ/kg·K
$\rho = 1000.0$	kg/m^3
$F = 1.38 \times 10^{-3}$	m^3/s
$C_{As} = 3.59$	kmol/m^3
$T_s = 388.57$	K
$C_{Ds} = 0.409$	kmol/m^3

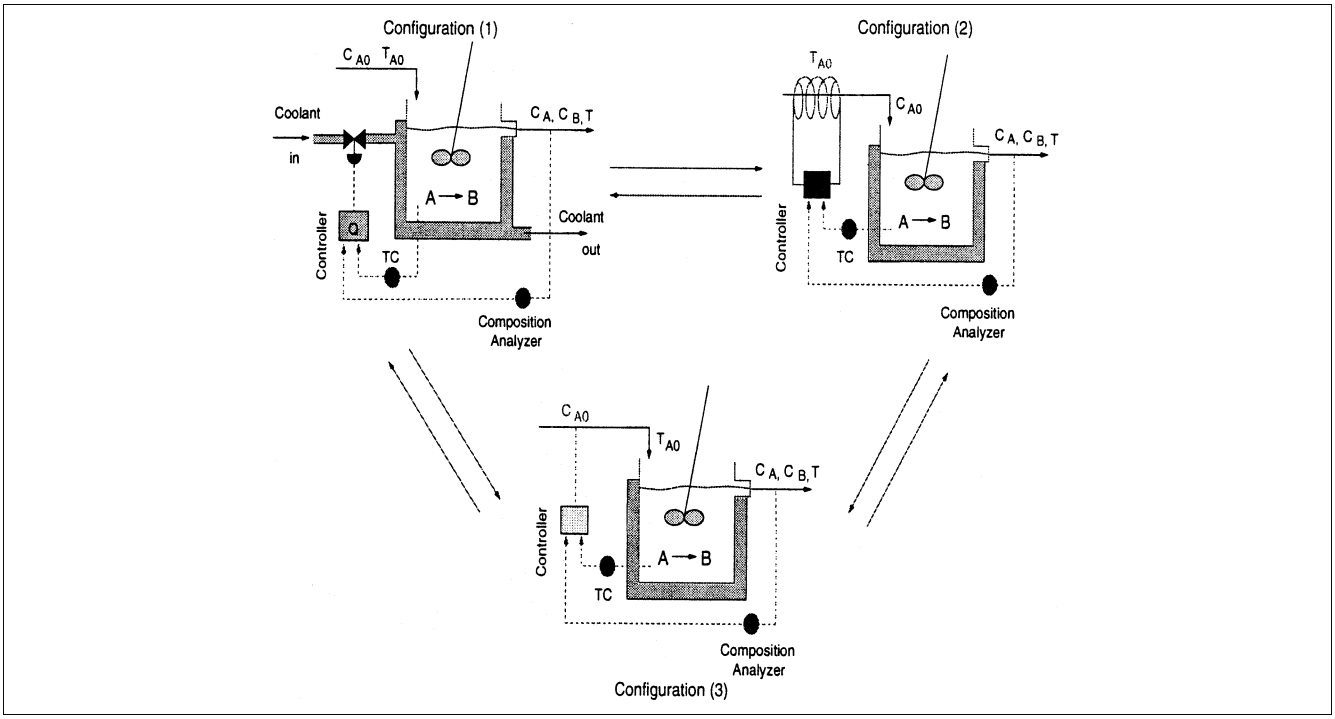

Figure 10. Switching between multiple control configurations, each characterized by a different manipulated input, provides a mechanism for fault-tolerant control.

(2) Inlet stream temperature, $u_2 = T_{A0} - T_{A0s}$, subject to the constraints $|u_2| \le u_2^{\max} = 100$ K.

(3) Inlet reactant concentration, $u_3 = C_{A0} - C_{A0s}$, subject to the constraints $|u_3| \le u_3^{\max} = 4$ kmol/m^3.

Each one of the preceding manipulated inputs represents a separate control configuration that, by itself, can stabilize the reactor at the desired steady state in the absence of faults. The first configuration, involving the heat input Q, will be taken as the primary control configuration. In the event of some failure in this configuration, however, the plant supervisor will have to activate one of the other two backup configurations in order to maintain closed-loop stability. The main question, which we use the hybrid control strategy to address, is how can the supervisor determine the appropriate backup control configuration to activate once failure is detected in the primary control configuration.

Controller Synthesis. Having identified the candidate control configurations that can be used, we outline in this section the main steps involved in the fault-tolerant control-system design procedure. These include (1) the synthesis of a stabilizing feedback controller for each control configuration, (2) the explicit characterization of the constrained stability region associated with each configuration, and (3) the design of a switching law that orchestrates the reconfiguration of the control system in a way that guarantees closed-loop stability in the event of failures in the active control configuration.

The first task involving the synthesis (for each control configuration) of a feedback controller that enforces asymptotic closed-loop stability in the presence of actuator constraints, is carried out on the basis of the process input/output dynamics. While our control objective is to achieve full state stabilization (and not output tracking), process outputs are introduced here only to facilitate transforming the system of Eq. 19 into a form more suitable for explicit controller synthesis. In the case of Eq. 19, a further simplification in controller design can be obtained by noting that the product concentration, C_B, does not influence the evolution of either the reactor temperature, T, or the reactant concentration, C_A, and, therefore, the controller design can be addressed solely on the basis of the T and C_A equations. A controller that stabilizes the (T,C_A) system will automatically stabilize the full system.

1. For the primary control configuration with $u_1 = Q$, we consider the output $y_1 = C_A - C_{As}$. This choice yields a relative degree of $r_1 = 2$ for the output with respect to the manipulated input. The coordinate transformation (in error variables form) takes the form

$$\begin{bmatrix} e_1 \\ e_2 \end{bmatrix} = \begin{bmatrix} C_A - C_{As} \\ \dfrac{F}{V}(C_{A0} - C_A) - \displaystyle\sum_{i=1}^{3} k_{i0} e^{-E_i/RT} C_A \end{bmatrix} \qquad (20)$$

2. For the second configuration with $u_2 = T_{A0} - T_{A0s}$, we choose the output $y_2 = C_A - C_{As}$, which yields the same relative degree as in the first configuration, $r_2 = 2$. The same coordinate transformation in Eq. 20 is obtained.

3. For the third configuration with $u_3 = C_{A0} - C_{A0s}$, we choose the output $y_3 = T - T_s$. This choice yields a relative degree $r_3 = 2$ of the output with respect to the manipulated input. The coordinate transformation in this case takes the

form

$$\begin{bmatrix} e_1 \\ e_2 \end{bmatrix} = \begin{bmatrix} T - T_s \\ \dfrac{F}{V}(T_{A0} - T) + \dfrac{Q}{\rho c_p V} + \displaystyle\sum_{i=1}^{3} \dfrac{(-\Delta H_i)}{\rho c_p} k_{i0} e^{-E_i/RT} C_A \end{bmatrix} \tag{21}$$

Note that since our objective is full state stabilization, the choice of the output in each of the preceding cases is really arbitrary. However, to facilitate our controller design and subsequent stability analysis, we have chosen in each case an output that produces a system of relative degree 2. For each configuration, the corresponding state transformation yields input/output dynamics of the following form

$$\begin{aligned} \dot{e} &= Ae + l_k(e) + b\alpha_k u_k, \qquad k = 1, 2, 3 \\ &:= \bar{f}_k(e) + \bar{g}_k(e) u_k \end{aligned} \tag{22}$$

where $A = \begin{bmatrix} 0 & 1 \\ 0 & 0 \end{bmatrix}$, $b = \begin{bmatrix} 0 \\ 1 \end{bmatrix}$, $l_k(\cdot) = L_{f_k}^2 h_k(x)$, $\alpha_k(\cdot) = L_{g_k} L_{f_k} h_k(x)$, $h_k(x) = y_k$ is the output associated with the kth configuration, $x = [x_1 \ x_2]^T$ with $x_1 = T - T_s$, $x_2 = C_A - C_{As}$, and the functions $f_k(\cdot)$ and $g_k(\cdot)$ can be obtained by rewriting the (T, C_A) model equations in Eq. 19 in the form of Eq. 1 for each configuration. The explicit forms of these functions are omitted for brevity. Using a common quadratic Lyapunov function of the form $V = e^T P e$, where

$$P = \begin{bmatrix} 1.7321 & 1 \\ 1 & 1.7321 \end{bmatrix}$$

is a positive definite symmetric matrix that satisfies the Riccati inequality of Eq. 18, we synthesize, for each control configuration, a bounded nonlinear feedback control law of the

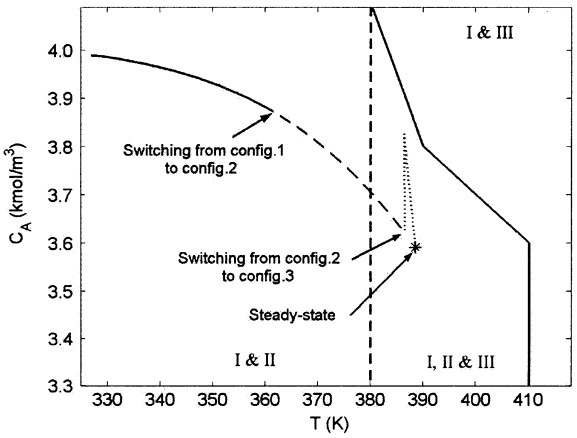

Figure 11. Stability regions for the Q-control configuration (I), the T_{A0}-control configuration (II), and the C_{A0}-control configuration (III).

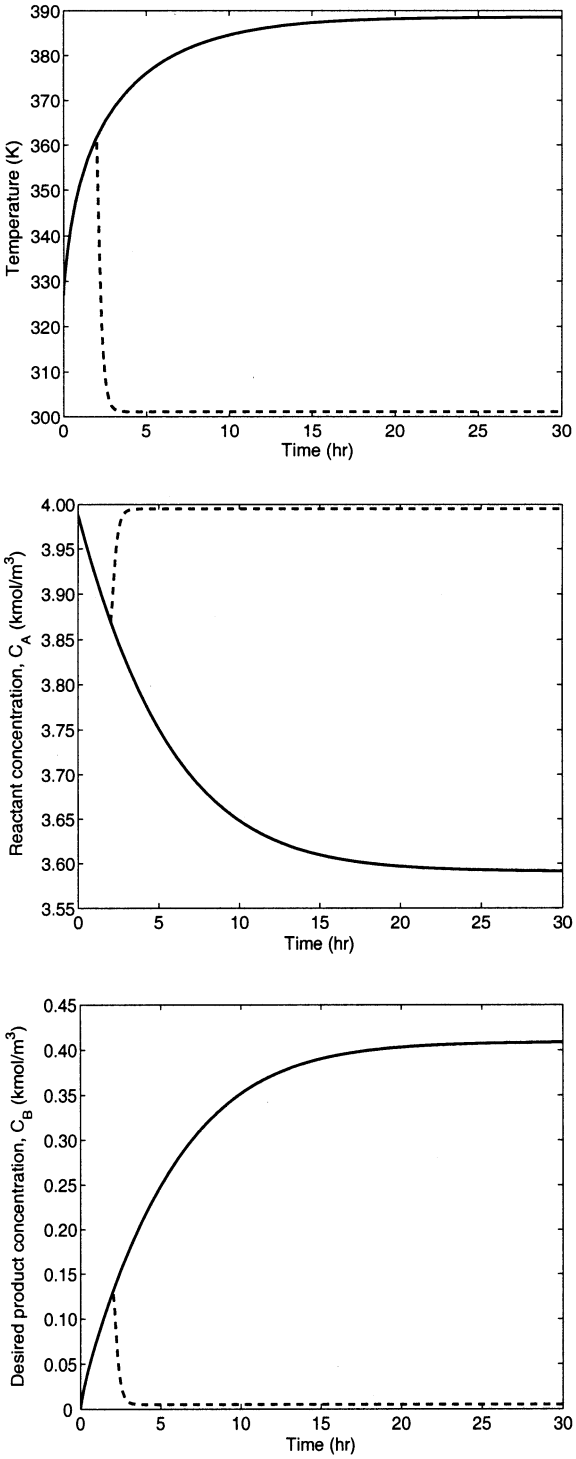

Figure 12. Evolution of the closed-loop temperature (top), reactant concentration (middle), and desired product concentration (bottom) profiles when the primary control configuration operates without failures (solid profiles), and when it fails at $t = 2.0$ h (dashed profiles) without activating any of the backup control configurations.

form

$$u_k = -\left(\frac{L^*_{\bar{f}_k}V + \sqrt{\left(L^*_{\bar{f}_k}V\right)^2 + \left(u_k^{\max}L_{\bar{g}_k}V\right)^4}}{\left(L_{\bar{g}_k}V\right)^2\left[1+\sqrt{1+\left(u_k^{\max}L_{\bar{g}_k}V\right)^2}\right]}\right)L_{\bar{g}_k}V \qquad (23)$$

where $L^*_{\bar{f}_k}V = L_{\bar{f}_k}V + \rho \| e \|^2, \rho > 0$, $k = 1, 2, 3$. An estimate of the constrained stability region, for each configuration, is then constructed by computing an invariant subset within the set $\Phi(u^k_{\max}) = \{x \in \mathbb{R}^2 : L^*_{\bar{f}_k}V \le u_k^{\max} \| L_{\bar{g}_k}V \|\}$, which is the set where the controller of the kth configurations respects the associated actuator constraints.

Closed-Loop Simulation Results. In this section, we demonstrate, through computer simulations, the implementation of the proposed fault-tolerant control methodology to the chemical reactor example introduced in Eq. 19. We have already described in the previous section how the feedback controllers are designed and the stability regions characterized for each of the three control configurations. Figure 11 depicts the stability region in the (T,C_A) space for each configuration. The stability region of the primary configuration (Q-configuration) covers the entire area of the plot. The stability region of the second configuration (T_{A0}-configuration) covers the entire area to the left of the solid line, while the stability region of the third configuration (C_{A0}-configuration) is the area to the right of the dashed vertical line. The desired steady state to be stabilized is shown with an asterisk that lies in the intersection of the three stability regions.

In the first set of simulation runs, we demonstrate the effect of actuator failure by comparing the closed-loop behavior when the control system operates with and without failures. To this end, the reactor is initialized at $T(0) = 327$ K, $C_A(0) = 3.99$ kmol/m^3, $C_B(0) = 0.0$ kmol/m^3 using the primary control configuration (with Q as the manipulated input). The solid profiles in Figures 12 and 13 depict the resulting temperature, reactant concentration, product concentration, and heat input profiles, respectively, when the control system operates without failures. It is seen in this case that the controller successfully stabilizes the reactor at the desired steady state. In contrast, the dashed profiles in the same figures show, respectively, the closed-loop state and manipulated input profiles, when the primary control configuration fails at $t = 2.0$ h (simulated by setting $Q = 0$ for all $t \ge 2.0$ h) and neither of the backup control configurations is activated at this time. It is clear that, in the absence of switching, the process reverts to its open-loop mode of operation and, thus, moves away from the desired steady-state.

To prevent closed-loop instability in the event of actuator failure, we implement, in the second set of simulation runs, the proposed hybrid control scheme. To this end, the reactor is initialized at the same initial condition, using the Q-control configuration, and the supervisor proceeds to monitor the evolution of the closed-loop trajectory. As shown by the solid parts of the closed-loop trajectory in Figure 11, the state profiles in Figure 14, and the heat input profile in Figure 15, the controller proceeds to drive the closed-loop trajectory toward the desired steady-state up until the Q-configuration fails after 2.0 h of reactor startup. From the solid part of the trajectory in the phase plot (Figure 11), it is clear that the failure

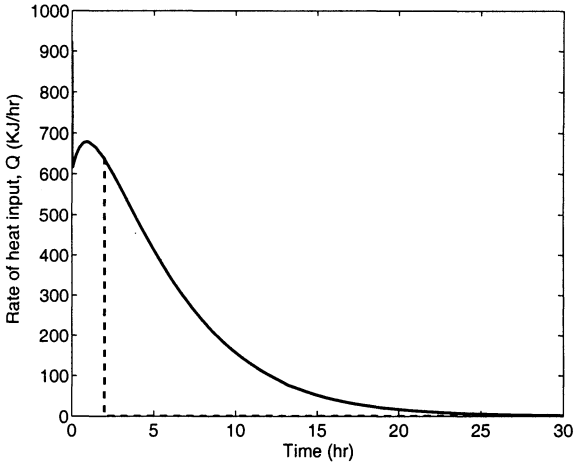

Figure 13. Rate of heat input profiles when the primary control configuration operates without failures (solid), and when it fails at $t = 2.0$ h (dashed) without activating any of the backup control configurations.

of the primary control configuration occurs when the closed-loop trajectory is within the stability region of the second control configuration and outside the stability region of the third control configuration. Therefore, on the basis of the switching logic of Eq. 11, the supervisor immediately activates the second configuration (with T_{A0} as the manipulated input). The result is shown by the dashed parts of the closed-loop trajectory in Figure 11, the state profiles in Figure 14, and the inlet stream temperature profile in Figure 15, where it is seen that, upon switching to the T_{A0}-configuration, the corresponding controller continues to drive the closed-loop trajectory closer to the desired steady state. Before reaching the steady state, however, we consider the case when a second failure occurs (this time in the T_{A0}-configuration) at $t = 15.0$ h (which is simulated by fixing T_{A0} for all $t \ge 15.0$ h). From the dashed part of the trajectory in Figure 11, it is clear that the failure of the second control configuration occurs when the closed-loop trajectory is within the stability region of the third configuration. Therefore, the supervisor immediately activates the third control configuration (with C_{A0} as the manipulated input), which finally stabilizes the reactor at the desired steady state (see the dotted parts of the closed-loop trajectory in Figure 11, the state profiles in Figure 14, and the inlet reactant concentration profile in Figure 15).

It is important to point out here that, if the second actuator failure were to occur outside the stability region of the third configuration, none of the available control configurations would be able to prevent closed-loop instability (unless the Q-configuration could somehow be repaired in time after its initial failure and then reactivated later). The resulting instability in this case would be due to the fundamental limitations imposed by constraints on the stability regions, as well as the fact that only three control configurations were considered in our simulations. In general, increasing the number of backup control configurations, together with increasing the maximum bounds on actuator capacity if possible, allows for greater flexibility in enforcing fault-tolerant control. In this

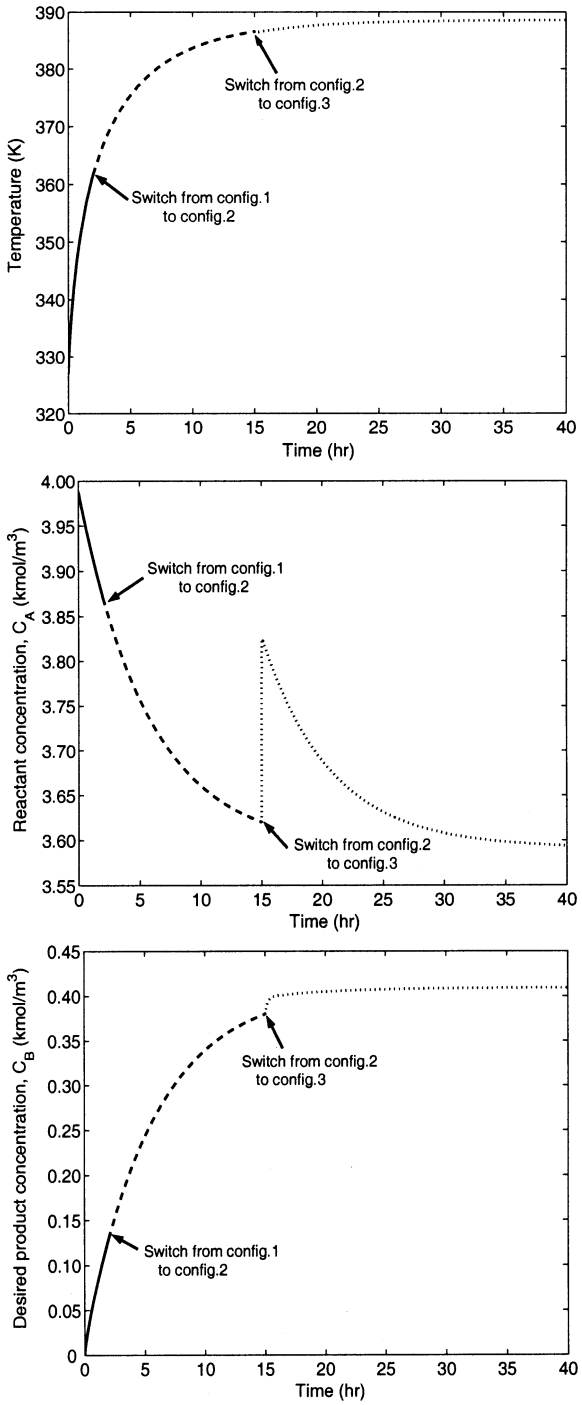

Figure 14. Evolution of the closed-loop temperature (top), reactant concentration (middle), and desired product concentration (bottom) profiles when the primary control configuration fails and the T_{A0}-control configuration is activated at $t = 2.0$ h, and when the T_{A0}-configuration fails and the C_{A0}-control configuration is activated at $t = 15$ h.

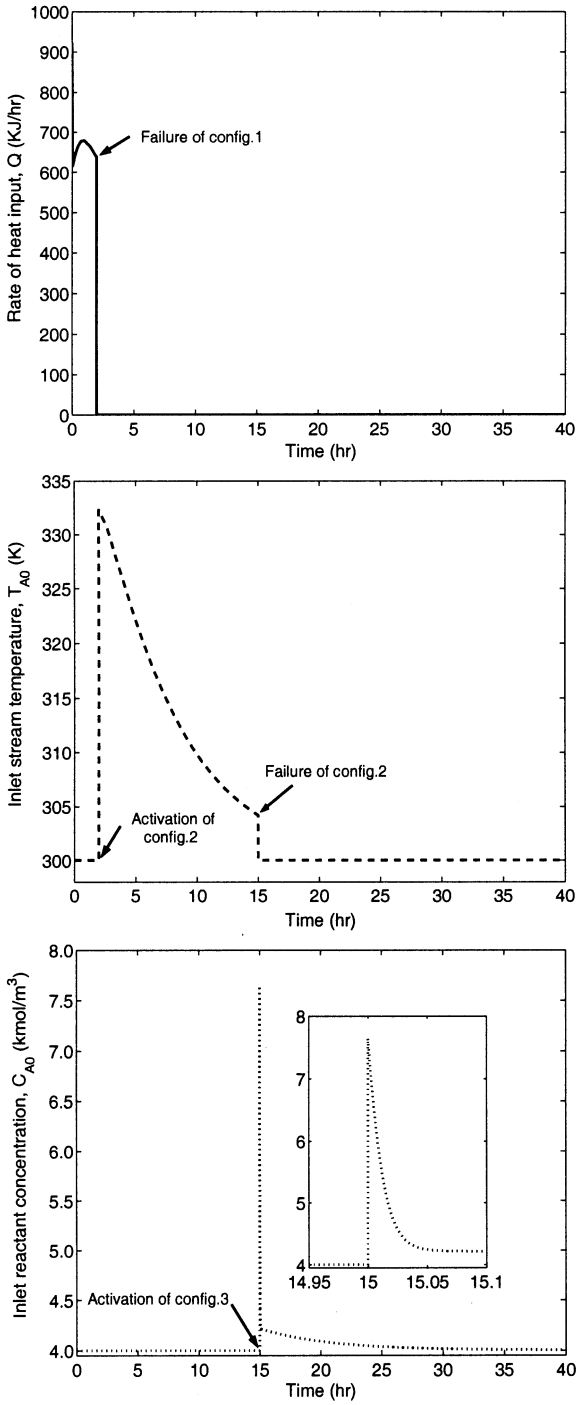

Figure 15. Manipulated input profiles under the Q-control configuration (top), the T_{A0}-control configuration (middle), and the C_{A0}-control configuration: T_{A0} starts to vary only after the first configuration fails at $t = 2.0$ h, while C_{A0} begins to vary after the second configuration fails at $t = 15$ h.

case, having larger, and more numerous, stability regions to switch between can reduce the possibility of failure occurring at a point when the trajectory is outside the stability region of every backup configuration. Such flexibility, however, is ultimately dependent on the physical limitations imposed by the process itself, such as the physical capacity of actuators, as well as the maximum number of control loops that can be

designed. In all of these cases, the hybrid control scheme, demonstrated earlier, provides valuable insight into the fault-tolerance limitations of a given control strategy, by indicating when a given failure can or cannot be tolerated by the control system.

Conclusions

In this work, a hybrid control strategy for a broad class of hybrid nonlinear processes with actuator constraints and model uncertainty was proposed. The control strategy coordinated, via multiple Lyapunov functions, the tasks of feedback-controller synthesis and logic-based switching between the constituent modes. A family of feedback controllers was designed to enforce robust stability within the constituent modes and provide an explicit characterization of the constrained region of robust stability for each mode. The stability regions were then used to derive stabilizing switching rules that orchestrate the transition between the various modes (and their controllers) in a way that guarantees robust stability for the overall hybrid process. The proposed hybrid-control method was applied through computer simulations to (1) robustly stabilize an exothermic chemical reactor, with switched dynamics, model uncertainty, and actuator constraints, at an unstable steady-state, and (2) design a fault-tolerant control system for chemical reactors through switching between multiple constrained control configurations.

Acknowledgment

Financial support, in part by NSF, CTS-0129571, and UCLA through a Chancellor's Fellowship, for N. H. El-Farra, is gratefully acknowledged. The authors also thank Adiwinata Gani for his assistance with the numerical simulations in the second example.

Literature Cited

Barton, P. I., and C. C. Pantelides, "Modeling of Combined Discrete/Continuous Processes," *AIChE J.*, **40**, 966 (1994).

Bemporad, A., and M. Morari, "Control of Systems Integrating Logic, Dynamics and Constraints," *Automatica*, **35**, 407 (1999).

Branicky, M. S., "Multiple Lyapunov Functions and Other Analysis Tools for Switched and Hybrid Systems," *IEEE Trans. Autom. Control*, **43**, 475 (1998).

DeCarlo, R. A., M. S. Branicky, S. Petterson, and B. Lennartson, "Perspectives and Results on the Stability and Stabilizability of Hybrid Systems," *Proc. IEEE*, **88**, 1069 (2000).

El-Farra, N. H., and P. D. Christofides, "Bounded Robust Control of Constrained Multivariable Nonlinear Processes," *Chem. Eng. Sci.*, **58**, 3025 (2003).

El-Farra, N. H., and P. D. Christofides, "Feedback Control of Switched Nonlinear Systems Using Multiple Lyapunov Functions," *Proc. American Control Conf.*, Arlington, VA, p. 3496 (2001a).

El-Farra, N. H., and P. D. Christofides, "Integrating Robustness, Optimality, and Constraints in Control of Nonlinear Processes," *Chem. Eng. Sci.*, **56**, 1841 (2001b).

El-Farra, N. H., and P. D. Christofides, "Switching and Feedback Laws for Control of Constrained Switched Nonlinear Systems," *Lecture Notes in Computer Science, Proc. of Int. Workshop on Hybrid Systems: Computation and Control*, Vol. 2289, C. J. Tomlin and M. R. Greenstreet, eds., Springer-Verlag, Berlin, p. 164 (2002).

Engell, S., S. Kowalewski, C. Schulz, and O. Stursberg, "Continuous-Discrete Interactions in Chemical Processing Plants," *Proc. IEEE*, **88**, 1050 (2000).

Freeman, R. A., and P. V. Kokotovic, *Robust Nonlinear Control Design: State-Space and Lyapunov Techniques*, Birkhauser, Boston (1996).

Grossmann, I. E., S. A. van den Heever, and I. Harjukoski, "Discrete Optimization Methods and Their Role in the Integration of Planning and Scheduling," *Proc. Int. Conf. on Chemical Process Control*, Tucson, AZ (2001).

Hespanha, J. P., and A. S. Morse, "Stability of Switched Systems with Average Dwell Time," *Proc. IEEE Conf. on Decision and Control*, Phoenix, AZ, p. 2655 (1999).

Hu, B., X. Xu, P. J. Antsaklis, and A. N. Michel, "Robust Stabilizing Control Law for a Class of Second-Order Switched Systems," *Syst. Contr. Lett.*, **38**, 197 (1999).

Isidori, A., *Nonlinear Control Systems: An Introduction, 3rd ed.*, Springer-Verlag, Berlin-Heidelberg (1995).

Khalil, H. K., *Nonlinear Systems*, 2nd ed., Macmillan, New York (1996).

Koutsoukos, X. D., P. J. Antsaklis, J. A. Stiver, and M. D. Lemmon, "Supervisory Control of Hybrid Systems," *Proc. IEEE*, **88**, 1026 (2000).

Lin, Y., and E. D. Sontag, "A Universal Formula for Stabilization with Bounded Controls," *Syst. Control Lett.*, **16**, 393 (1991).

Sepulchre, R., M. Jankovic, and P. Kokotovic, *Constructive Nonlinear Control*, 1st ed., Springer-Verlag, Berlin Heidelberg (1997).

Sontag, E. D., "Smooth Stabilization Implies Corprime Factorization," *IEEE Trans. Autom. Control*, **34**, 435 (1989).

Yamalidou, E. C., and J. Kantor, "Modeling and Optimal Control of Discrete-Event Chemical Processes Using Petri Nets," *Comput. Chem. Eng.*, **15**, 503 (1990).

Appendix A: Proof of Theorem 1

To prove this theorem, we proceed in two steps. In the first step we show that, for each individual mode (without switching), the control law of Eqs. 7–9 satisfies the constraints within the region described by Eq. 10 and that, starting from any initial condition within the set Ω_i^*, the corresponding feedback-control law robustly asymptotically stabilizes the ith closed-loop subsystem. In the second step, we use this fact together with MLF stability analysis to show that the switching laws of Eqs. 11–12 enforce asymptotic stability in the switched uncertain closed-loop system, starting from any initial condition that belongs to any of the sets Ω_i^*, $i \in \mathfrak{I}$.

Step 1. To prove that the control law of Eqs. 7–9 satisfies the constraints within the region described by the inequality of Eq. 10, we need consider only the case when $\|(L_{G_i}V_i)^T\| \neq 0$ (since when $\|(L_{G_i}V_i)^T\| = 0$, $u_i = 0$ and the constraints are trivially satisfied). For this case, we have from Eqs. 7 and 8

$$\|u_i(x)\| \leq \|k_i(V_i, u_i^{\max}, \theta_{bi}, \chi_i, \phi_i)\| \, \|\left(L_{G_i}V_i\right)^T\| \leq \frac{\left\| L_{f_i}^* V_i + \sqrt{\left(L_{f_i}^{**}V_i\right)^2 + \left(u_i^{\max}\|\left(L_{G_i}V\right)^T\|\right)^4} \right\|}{\left\|\left(L_{G_i}V_i\right)^T\right\| \left[1 + \sqrt{1 + \left(u_i^{\max}\|\left(L_{G_i}V_i\right)^T\|\right)^2}\right]} \tag{A1}$$

From the definitions of $L_{f_i}^* V_i$ and $L_{f_i}^{**} V_i$ in Eq. 9 and the fact that $\rho > 0$, it is clear that if $L_{f_i}^{**} V_i \leq u_i^{\max}\|(L_{G_i}V_i)^T\|$, then we also have $L_{f_i}^* V_i \leq u_i^{\max}\|(L_{G_i}V_i)^T\|$. Therefore, for any x satisfying Eq. 10, the following estimates hold

$$\left(L_{f_i}^{**}V_i\right)^2 \leq \left(u_i^{\max}\|\left(L_{G_i}V_i\right)^T\|\right)^2$$

$$L_{f_i}^* V_i \leq u_i^{\max}\|\left(L_{G_i}V_i\right)^T\| \tag{A2}$$

Substituting the preceding estimates into Eq. A1 yields

$$\| u_i(x) \| \leq \frac{u_i^{\max} \left\| \left(L_{G_i} V_i \right)^T \right\| \left[1 + \sqrt{1 + \left(u_i^{\max} \| \left(L_{G_i} V_i \right)^T \| \right)^2} \right]}{\left\| \left(L_{G_i} V_i \right)^T \right\| \left[1 + \sqrt{1 + \left(u_i^{\max} \| \left(L_{G_i} V_i \right)^T \| \right)^2} \right]} = u_i^{\max} \tag{A3}$$

which shows that the constraints are satisfied. Consider now the ith subsystem of the switched nonlinear system of Eq. 1. Substituting the control law of Eqs. 7–9, evaluating the time derivative of the Lyapunov function along the closed-loop trajectories, and using the fact that $\| (L_{G_i} V_i)^T \|^2 = (L_{G_i} V_i)(L_{G_i} V_i)^T$, we obtain

$$\begin{aligned} \dot{V}_i &= L_{f_i} V_i + L_{G_i} V_i u_i + L_{W_i} V_i \theta_i \\ &= L_{f_i} V_i + L_{W_i} V_i \theta_i + L_{G_i} V_i \\ &\times \left(\frac{L_{f_i}^* V_i + \sqrt{\left(L_{f_i}^{**} V_i \right)^2 + \left(u_i^{\max} \| \left(L_{G_i} V_i \right)^T \| \right)^4}}{\| \left(L_{G_i} V_i \right)^T \|^2 \left[1 + \sqrt{1 + \left(u_i^{\max} \| \left(L_{G_i} V_i \right)^T \| \right)^2} \right]} \right) \left(L_{G_i} V_i \right)^T \\ &\leq L_{f_i} V_i + \chi_i \| L_{W_i} V_i \| \theta_{bi} \\ &- \left(\frac{L_{f_i}^* V_i + \sqrt{\left(L_{f_i}^{**} V_i \right)^2 + \left(u_i^{\max} \| \left(L_{G_i} V_i \right)^T \| \right)^4}}{\| \left(L_{G_i} V_i \right)^T \|^2 \left[1 + \sqrt{1 + \left(u_i^{\max} \| \left(L_{G_i} V_i \right)^T \| \right)^2} \right]} \right) \end{aligned} \tag{A4}$$

After performing some algebraic manipulations, the preceding inequality can be rewritten as

$$\dot{V}_i \leq \alpha_i(x) + \left(\frac{\theta_{bi} \| L_{W_i} V_i \| \left(\dfrac{\phi_i - (\chi - 1) \| x \|}{\| x \| + \phi_i} \right) - \rho_i \left(\dfrac{\| x \|^2}{\| x \| + \phi_i} \right)}{\left[1 + \sqrt{1 + \left(u_i^{\max} \| \left(L_{G_i} V_i \right)^T \| \right)^2} \right]} \right) \tag{A5}$$

where

$$\alpha_i(x) = \left(\frac{\left(L_{f_i} V_i + \chi_i \theta_{bi} \| L_{W_i} V_i \| \right) \sqrt{1 + \left(u_i^{\max} \| \left(L_{G_i} V_i \right)^T \| \right)^2} - \sqrt{\left(L_{f_i}^{**} V_i \right)^2 + \left(u_i^{\max} \| \left(L_{G_i} V_i \right)^T \| \right)^4}}{\left[1 + \sqrt{1 + \left(u_i^{\max} \| \left(L_{G_i} V_i \right)^T \| \right)^2} \right]} \right) \tag{A6}$$

To analyze the sign of $\dot{V}_i$ in Eq. A5, we initially study the sign of the term $\alpha_i(x)$, on the righthand side. It is clear that the sign of this term depends on the sign of the term $L_{f_i} V_i + \chi_i \| L_{W_i} V_i \| \theta_{bi}$. To this end, we consider the following two cases.

Case 1: $L_{f_i}^{**} V_i \leq 0$. Since $L_{f_i}^{**} V_i = L_{f_i} V_i + \rho_i \| x \| + \chi_i \| L_{W_i} V_i \| \theta_{bi}$ and ρ_i is a positive real number, the fact that $L_{f_i}^{**} V_i \leq 0$ implies that $L_{f_i} V_i + \chi_i \| L_{W_i} V_i \| \theta_{bi} \leq 0$. As a result, we have that $\alpha_i(x) \leq 0$, and the time derivative of V_i in this case satisfies the following bound

$$\dot{V}_i \leq \left(\frac{\| L_{W_i} V_i \| \theta_{bi} \left(\dfrac{\phi_i - (\chi_i - 1) \| x \|}{\| x \| + \phi_i} \right) - \rho_i \left(\dfrac{\| x \|^2}{\| x \| + \phi_i} \right)}{\left[1 + \sqrt{1 + \left(u_i^{\max} \| \left(L_{G_i} V_i \right)^T \| \right)^2} \right]} \right) \equiv \beta_i(x) \tag{A7}$$

Case 2: $0 < L_{f_i}^{**} V_i \leq u_i^{\max} \| (L_{G_i} V_i)^T \|$. In this case, we have

$$\left(L_{f_i}^{**} V_i \right)^2 \leq \left(u_i^{\max} \| \left(L_{G_i} V_i \right)^T \| \right)^2 \tag{A8}$$

and, therefore

$$\begin{aligned} &- \sqrt{\left(L_{f_i}^{**} V_i \right)^2 + \left(u_i^{\max} \| \left(L_{G_i} V_i \right)^T \| \right)^4} \\ &= - \sqrt{\left(L_{f_i}^{**} V_i \right)^2 + \left(u_i^{\max} \| \left(L_{G_i} V_i \right)^T \| \right)^2 \left(u_i^{\max} \| \left(L_{G_i} V_i \right)^T \| \right)^2} \\ &\leq - \left(L_{f_i}^{**} V_i \right) \sqrt{1 + \left(u_i^{\max} \| \left(L_{G_i} V_i \right)^T \| \right)^2} \end{aligned} \tag{A9}$$

Substituting the estimate of Eq. A9 in the expression for $\dot{V}_i$ in Eqs. A5–A6 yields

$$\begin{aligned} \dot{V}_i &= \frac{- \rho_i \| x \| \sqrt{1 + \left(u_i^{\max} \| \left(L_{G_i} V_i \right)^T \| \right)^2}}{\left[1 + \sqrt{1 + \left(u_i^{\max} \| \left(L_{G_i} V_i \right)^T \| \right)^2} \right]} + \beta_i(x) \\ &\leq \beta_i(x) \end{aligned} \tag{A10}$$

From the preceding analysis, it is clear that whenever $L_{f_i}^{**} V_i \leq u_i^{\max} \| (L_{G_i} V_i)^T \|$, the inequality of Eq. A7 holds. Since $\Omega_i^*(u_i^{\max}, \theta_{bi})$ is taken to be the largest invariant set embedded within the region described by Eq. 10, we have that starting from any $x(0) \in \Omega_i^*$, the inequality of Eq. A7 holds. Referring to this inequality, note that since $\chi_i > 1$ and $\rho_i > 0$, it is clear that whenever $\| x \| > \phi_i / (\chi_i - 1)$, the first term on

the righthand side is strictly negative, and therefore $\dot{V}_i$ satisfies

$$\dot{V}_i \le -\frac{\rho_i \|x\|^2}{(\|x\|+\phi_i)\left[1+\sqrt{1+\left(u_i^{\max}\|\left(L_{G_i}V_i\right)^T\|\right)^2}\right]} \quad \text{(A11)}$$

To study the behavior of $\dot{V}_i$ when $\|x\| \le \phi_i/(\chi_i - 1)$, we first note that since the entries of the matrix function $W_i(x)$ and the entries of the row vector $\nabla_x V_i$ are smooth and vanish when $x = 0$, then there exists positive real constants ϕ_i^1, δ_i, δ_i' such that if $\phi_i \le \phi_i^1$, the bounds $\|W_i(x)\| \le \delta_i\|x\|$, $\|\nabla_x^T V_i\| \le \delta_i' \|x\|$ hold for $\|x\| \le \phi_i/(\chi_i - 1)$. Using this bound, we obtain the following estimates

$$\begin{aligned}\|L_{W_i}V_i\|\theta_{bi}(\phi_i - (\chi_i - 1)\|x\|) &\le \|L_{W_i}V_i\|\theta_{bi}\phi_i \\ &\le \|W_i(x)\|\,\|\nabla_x^T V_i\|\theta_{bi}\phi_i \\ &\le \phi_i\theta_{bi}\delta_i\delta_i'\|x\|^2 \qquad \forall \|x\| \le \frac{\phi_i}{\chi_i - 1}\end{aligned} \quad \text{(A12)}$$

Substituting the estimate of Eq. A12 directly into Eq. A7, we get

$$\dot{V}_i \le \left(\frac{(\phi_i\theta_{bi}\delta_i\delta_i' - \rho_i)\|x\|^2}{(\|x\|+\phi_i)\left[1+\sqrt{1+\left(u_i^{\max}\|\left(L_{G_i}V_i\right)^T\|\right)^2}\right]}\right) \quad \forall \|x\| \le \frac{\phi_i}{\chi_i - 1} \quad \text{(A13)}$$

If ϕ_i is sufficiently small to satisfy the bound $\phi_i \le \rho_i/(2\theta_{bi}\delta_i\delta_i')' \equiv \phi_i^2$, then it is clear from Eqs. A11–A13 that $\dot{V}_i < 0 \forall \times \ne 0$. In summary, we have that for any initial condition in the invariant set Ω_i^*, there exists $\phi_i^* \equiv \min\{\phi_i^1, \phi_i^2\}$ such that if $\phi_i \le \phi_i^*$, $\dot{V}_i$ satisfies

$$\dot{V} \le \frac{-\rho_i'\|x\|^2}{(\|x\|+\phi_i)\left[1+\sqrt{1+\left(u_i^{\max}\|\left(L_{G_i}V_i\right)^T\|\right)^2}\right]} < 0 \quad \forall x \ne 0, \qquad i = 1, \ldots, N \quad \text{(A14)}$$

where $\rho_i' = \rho_i/2$, which implies that the individual closed-loop subsystems are asymptotically stable.

Step 2. Consider now the switched closed-loop system and, without loss of generality, suppose that $x(0) \in \Omega_i^*$ for some $i \in \mathfrak{I}$. Then it follows from Eq. A14 and the invariance of Ω_i^* that the Lyapunov function for this mode, V_i, decays monotonically along the trajectories of the closed-loop system for as long as mode i is to remain active, that is, for all times such that $\sigma(t) = i$. If at any time, T, such that $x(T) \in \Omega_j^*$ for some $j \in \mathfrak{I}$, $j \ne i$, we set $\sigma(T^+) = j$ (that is, activate mode j and its respective controller), then using the same argument, it is clear that the corresponding Lyapunov function for this mode, V_j, will also decay monotonically for as long as we keep $\sigma(t) = j$. Note that T, which is the time that mode i is switched out, is not known *a priori*, but is rather determined by the evolution of the closed-loop continuous state. By tracking the closed-loop trajectory in this manner, we conclude that, starting from any $x(0) \in \Omega_i^*$ for any $i \in \mathfrak{I}$ and as long as the ith mode (and its controller) is activated only at a time when $x(t) \in \Omega_i^*$, we have that for all $i \in \mathfrak{I}$, $k \in Z_+$

$$\dot{V}_{\sigma(t_{i_k})} < 0 \qquad \forall t \in \left[t_{i_k}, t_{i_k'}\right) \quad \text{(A15)}$$

where t_{i_k} and $t_{i_k'}$ refer, respectively, to the times that the i-th mode is switched in and out for the kth time by the supervisor. Furthermore, from Eq. 12 we have that for any admissible switching time t_{i_k}

$$V_i\left[x\left(t_{i_k}\right)\right] < V_i\left[x\left(t_{i_{k-1}'}\right)\right] \quad \text{(A16)}$$

which consequently implies that

$$V_i\left[x\left(t_{i_k}\right)\right] < V_i\left[x\left(t_{i_{k-1}}\right)\right] \quad \text{(A17)}$$

since $V_i(x(t_{i_{k-1}'})) < V_i(x(t_{i_{k-1}}))$ from Eq. A15. Using Eqs. A15–A17, a direct application of the MLF result of Theorem 2.3 in Branicky (1998) can be performed to conclude that the switched closed-loop system is Lyapunov stable under the switching laws of Theorem 1. To prove asymptotic stability, we note that Eq. A16 also implies

$$V_i\left(x\left(t_{i_k'}\right)\right) < V_i\left(x\left(t_{i_{k-1}'}\right)\right) \quad \text{(A18)}$$

since $V_i(x(t_{i'k})) < V_i(x(t_{i_k}))$ from Eq. A15. From the strict inequality in Eq. A18, it follows that for every (infinite) sequence of switching times $t_{i_1'}$, $t_{i_2'}$, … such that $\sigma(t_{i_k}^+) = \sigma(t_{i_k}^-) = i$, the sequence $V_{\sigma(t_{i_1'})}$, $V_{\sigma(t_{i_2'})}$, … is decreasing and positive, and, therefore, has a limit $L \ge 0$. We have

$$\begin{aligned}0 = L - L &= \lim_{k\to\infty} V_{\sigma(t_{i'k+1}^-)}\left[x\left(t_{i_{k+1}'}\right)\right] - \lim_{k\to\infty} V_{\sigma(t_{i_k'}^-)}\left[x\left(t_{i_k'}\right)\right] \\ &= \lim_{k\to\infty}\left\{V_i\left[x\left(t_{i_{k+1}'}\right)\right] - V_i\left[x\left(t_{i_k'}\right)\right]\right\}\end{aligned} \quad \text{(A19)}$$

Note that the argument of the limit in the preceding equation is strictly negative for all nonzero x and zero only when $x = 0$ (from Eq. A18). Therefore, there exists a function α of class $\mathcal{K}$ (that is, continuous, increasing, and zero at zero) such that

$$V_i\left[x\left(t_{i_{k+1}'}\right)\right] - V_i\left[x\left(t_{i_k'}\right)\right] \le -\alpha\left(\|x\left(t_{i_k'}\right)\|\right) \quad \text{(A20)}$$

Substituting the preceding estimate into Eq. A19, we have

$$\begin{aligned}0 &= \lim_{k\to\infty}\left\{V_i\left[x\left(t_{i_{k+1}'}\right)\right] - V_i\left[x\left(t_{i_k'}\right)\right]\right\} \\ &\le \lim_{k\to\infty}\left[-\alpha\left(\|x\left(t_{i_k'}\right)\|\right)\right] \le 0\end{aligned} \quad \text{(A21)}$$

which implies that $x(t)$ converges to the origin, which together with Lyapunov stability, implies that the switched closed-loop system is asymptotically stable. This concludes the proof of the theorem.

Appendix B: Proof of Theorem 2

The proof of this theorem shares several steps with the proof of Theorem 1. We will highlight only the differences.

Step 1. We have already shown in step 1 of the proof of Theorem 1 that, for each mode considered separately, the evolution of the corresponding Lyapunov function, starting from any $x(0) \in \Omega_i^*$, obeys the growth bound of Eq. A11 whenever $\|x\| \geq \phi_i/(\chi_i - 1)$. Since the uncertain variables are nonvanishing, the bounds used in Eq. A12 to establish asymptotic convergence to the origin cannot be invoked here, and no further conclusion can be made regarding the sign of $\dot{V}_i$ when $\|x\| < \phi_i/(\chi_i - 1)$. However, from Eq. A12, we conclude that $\dot{V}_i$ is negative-definite outside a ball of radius $\epsilon_i = \phi_i/(\chi_i - 1)$, which implies [see Theorem 5.1 and its corollaries in Khalil (1996)] that, for any $x(0) \in \Omega_i^*$, there exists a finite time t_1 such that the solution to the ith closed-loop system satisfies

$$\begin{aligned} \|x(t)\| &\leq \beta_i(\|x_0\|, t), \qquad \forall \quad 0 \leq t < t_1 \\ \|x(t)\| &\leq b_i(\epsilon_i), \qquad \forall \quad t \geq t_1 \end{aligned} \tag{B1}$$

where $\beta_i(\cdot,\cdot)$ is a class $\mathcal{KL}$ function and $b_i(\cdot)$ is of class $\mathcal{K}_\infty$. This implies that the state is ultimately bounded and that the ultimate bound can be made arbitrarily small by choosing ϵ_i to be sufficiently small.

Step 2. Having established boundedness of the trajectory of the individual closed-loop modes of the hybrid system, we proceed in this step to show boundedness of the overall switched closed-loop trajectory. To this end, given any positive real number d, it follows, from the properties of class $\mathcal{K}_\infty$ functions, that there exist a set of positive real numbers, $\{\epsilon_1^*, \epsilon_2^*, \ldots, \epsilon_N^*\}$ such that

$$b_1(\epsilon_1^*) = b_2(\epsilon_2^*) = \cdots = b_N(\epsilon_N^*) \leq d \tag{B2}$$

where $\epsilon_i^* \geq \epsilon_i \forall i \in \mathcal{I}$ which ensures that all modes share a common residual set. Since switching occurs only in regions where the various stability regions intersect (as required by Eq. 11), we need consider only the case when the intersection, $\bigcap_i \Omega_i^*$, is nonempty and choose d such that the set $D = \{x \in \mathbb{R}^n : \|x\| \leq d\} \subset \bigcap_i \Omega_i^*$, $i = 1, \ldots, N$.

Without loss of generality, assume that $x(0) \in \Omega_i^*$ for some $i \in \mathcal{I}$. If this mode remains active for all times, then boundedness follows directly from the analysis in step 1. If switching takes place, however, then it follows from the switching rules of Eqs. 11 and 12 that for every admissible sequence of switching times, $t_{i_1}, t_{i_2}, \ldots$, such that $\sigma(t_{i_k}^+) = i$ and $\|x(t_{i_k})\| > d$, the positive sequence $V_{\sigma(t_{i_1})}, V_{\sigma(t_{i_2})}, \cdots$, is monotonically decreasing. This, together with the fact that the set D is nonempty and completely contained within $\bigcap_i \Omega_i^*$, implies the existence of a finite k^* such that $\|x(t_{i_k})\| \leq d$ for some $k \geq k^*$, $k \in Z_+$. Since N is finite, and only a finite number of switches are allowed over any finite time interval, the preceding analysis implies that, if $\epsilon_i \leq \epsilon_i^*$, $\forall i \in \mathcal{I}$, then there exists finite time, t', during which (at least) one of the modes will converge to D. Since D was chosen to be a common residual set for all the modes (Eq. B2), it follows that $\|x(t)\| \leq d$ for all $t \geq t'$, regardless of which mode is switched in or out for $t \geq t'$. Therefore, the switched closed-loop trajectory is bounded for all times. This concludes the proof of the theorem.

Manuscript received May 31, 2002, revision received Jan. 10, 2003, and final revision received Mar. 11, 2003.